

# UPCommons

## Portal del coneixement obert de la UPC

<http://upcommons.upc.edu/e-prints>

The version of record of this article, first published in *CEAS Space Journal*, is available online at Publisher's website: <https://doi.org/10.1007/s12567-022-00434-3>.



# A method for the experimental characterisation of novel drag-reducing materials for very low Earth orbits using the Satellite for Orbital Aerodynamics Research (SOAR) mission

Nicholas H. Crisp<sup>1</sup> · Peter C. E. Roberts<sup>1</sup> · Virginia Hanessian<sup>2</sup> · Valeria Sullioti-Linner<sup>3</sup> · Georg H. Herdrich<sup>4</sup> · Daniel García-Almiñana<sup>5</sup> · Dhiren Kataria<sup>6</sup> · Simon Seminari<sup>7</sup>

Received: 15 September 2021 / Revised: 11 February 2022 / Accepted: 13 February 2022  
© The Author(s) 2022

## Abstract

The Satellite for Orbital Aerodynamics Research (SOAR) is a 3U CubeSat mission that aims to investigate the gas–surface interactions (GSIs) of different materials in the very low Earth orbit environment (VLEO), i.e. below 450 km. Improving the understanding of these interactions is critical for the development of satellites that can operate sustainably at these lower orbital altitudes, with particular application to future Earth observation and communications missions. SOAR has been designed to perform the characterisation of the aerodynamic coefficients of four different materials at different angles of incidence with respect to the flow and at different altitudes in the VLEO altitude range. Two conventional and erosion-resistant materials (borosilicate glass and sputter-coated gold) have first been selected to support the validation of the ground-based Rarefied Orbital Aerodynamics Research (ROAR) facility. Two further, novel materials have been selected for their potential to reduce the drag experienced in orbit whilst also remaining resistant to the detrimental effects of atomic oxygen erosion in VLEO. In this paper, the uncertainty associated with the experimental method for determining the aerodynamic coefficients of satellite with different configurations of the test materials from on-orbit data is estimated for different assumed gas–surface interaction properties. The presented results indicate that for reducing surface accommodation coefficients the experimental uncertainty on the drag coefficient determination generally increases, a result of increased aerodynamic attitude perturbations. This effect is also exacerbated by the high atmospheric density at low orbital altitude (i.e. 200 km), resulting in high experimental uncertainty. Co-rotated steerable fin configurations are shown to provide generally lower experimental uncertainty than counter-rotated configurations, with the lowest uncertainties expected in the mid-VLEO altitudes (~300 km). For drag coefficient experiments, configurations with two fins oriented at 90° were found to allow the best differentiation between surfaces with different GSI performance. In comparison, the determination of the lift coefficient is found to be improve as the altitude is reduced from 400 to 200 km. These experiments were also found to show the best expected performance in determining the GSI properties of different materials. SOAR was deployed into an orbit of 421 km × 415 km with 51.6° inclination on 14 June 2021. This orbit will naturally decay allowing access to different altitudes over the lifetime of the mission. The results presented in this paper will be used to plan the experimental schedule for this mission and to maximise the scientific output.

**Keywords** Very low Earth orbit (VLEO) · Orbital aerodynamics · Drag and lift coefficient · Gas–surface interactions (GSIs) · CubeSat

✉ Nicholas H. Crisp  
nicholas.crisp@manchester.ac.uk

<sup>1</sup> The University of Manchester, Oxford Road,  
Manchester M13 9PL, UK

<sup>2</sup> GomSpace A/S, Langagervej 6, 9220 Aalborg East, Denmark

<sup>3</sup> Elecnor Deimos Satellite Systems, C/Francia 9,  
13500 Puertollano, Spain

<sup>4</sup> Institute of Space Systems (IRS), University of Stuttgart,  
Pfaffenwaldring 29, 70569 Stuttgart, Germany

<sup>5</sup> UPC-BarcelonaTECH, Colom 11, TR5, 08222 Terrassa,  
Spain

<sup>6</sup> Mullard Space Science Laboratory, University College  
London, Holmbury St. Mary, Dorking, Surrey RH5 6NT, UK

<sup>7</sup> Euroconsult, 86 Boulevard de Sébastopol, Paris, France

## 1 Introduction

A reduction in the operational orbit altitude of spacecraft has been linked to a number of benefits to their design, particularly for Earth observation (EO) [1] and communications missions [2]. Interest in use of very low Earth orbits (VLEO), those below 450 km in altitude, has recently grown correspondingly for such applications. However, critical challenges to the sustained operation of spacecraft in VLEO exist. Most importantly, the atmosphere is significantly denser in VLEO and increases with reducing altitude. The aerodynamic drag experienced by spacecraft in VLEO is therefore increased and the natural lifetime before de-orbit and demise is much shorter than from higher, traditional LEO altitudes. To increase the orbital lifetime, the experienced drag can be counteracted directly by thrust forces generated by a propulsion system, i.e. drag compensation. Drag mitigation can also be performed with the aim of reducing the magnitude of the drag experienced, principally by considering the design of the geometry of the spacecraft and the interaction of the external surfaces with the oncoming atmospheric flow [3].

At VLEO altitudes the atmospheric density is many orders of magnitude lower than at the ground, as shown in Fig. 1, and is, therefore, highly rarefied. For such conditions, the Knudsen number  $Kn$ , defined as the ratio between the mean free path of the atmospheric particles  $\lambda$  and a characteristic length  $L$ , can be used to define the flow regime. For an orbiting spacecraft of a typical size, the Knudsen number is large ( $Kn \gg 10$ ) and free-molecular flow (FMF) conditions apply, effectively meaning that the interactions between gas particles and the spacecraft surfaces are more frequent and of greater significance than

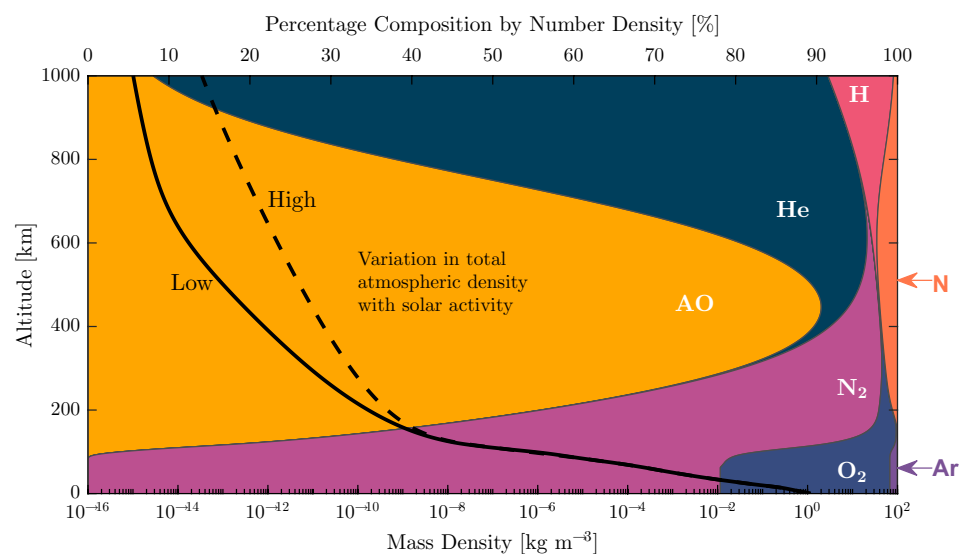
interactions between the gas particles themselves, including those reflected or re-emitted from the surfaces.

Under such conditions, the aerodynamic forces experienced are determined by the exchange in momentum between the oncoming atmospheric flow and the external spacecraft surfaces. The nature of the interaction of the oncoming atmospheric particles with an incident surface and their subsequent velocity and distribution following scattering are principally control the momentum exchange. As a result, these gas–surface interactions (GSIs) are predominantly responsible for the aerodynamic forces experienced by surfaces in VLEO [6, 7].

When considering the momentum exchange occurring on a given surface, two extreme modes of GSI are typically defined: specular reflection and diffuse re-emission. In the case of specular reflection, no thermal energy is transferred to the surface and the particle is elastically reflected from the surface. The momentum exchange therefore only occurs along the surface normal vector. Comparatively, for diffuse re-emission the incident particle is thermally equilibrated with the surface and the subsequent re-emission has a probabilistic velocity and angular distribution based on the surface temperature. A broad range of different scattering dynamics have the potential to exist between these two extremes and may apply under different conditions.

GSI behaviour in LEO has been considered to be affected by a number of factors, including the composition, structure, roughness and contamination of the surface, and the temperature, composition, velocity, and incidence angle of the oncoming flow [8–10]. However, despite this range of parameters, historical analysis of spacecraft orbiting in LEO has suggested that diffuse re-emission characteristics are dominant, particularly for spacecraft surfaces below 200 km in altitude [11, 12]. These effects have been attributed due to the high concentration of atomic oxygen (AO)

**Fig. 1** Representative variation of atmospheric density and composition with altitude in LEO, calculated using the NRLMSISE-00 model [4]. Solar activity and geomagnetic index defined as per ISO 14222:2013 [5]



present in LEO altitudes (see Fig. 1) that adsorbs to and erodes the external spacecraft surfaces. The interactions with the roughened and contaminated surfaces mean that significant energy is transferred from the flow to the spacecraft and largely diffuse and thermal particle re-emission is observed. As a result of this GSI behaviour the magnitude of the drag force is large and the lift force production is comparatively small (an order of magnitude less than the drag) [13]. This GSI behaviour has been measured experimentally at an altitude of 225 km, showing almost completely diffuse re-emission and high accommodation [14].

The role of speed ratio  $s$  is also an important factor when considering spacecraft aerodynamics and can be defined as the ratio between the bulk velocity of the flow  $v_\infty$  and the most probably thermal velocity  $v_{th}$  of the gas particles assuming a Maxwellian velocity distribution

$$s = \frac{v_\infty}{v_t} = \frac{v_\infty}{\sqrt{\frac{2k_B T}{m_m}}}, \quad (1)$$

where  $k_B$  is the Boltzmann constant,  $T$  is the atmospheric temperature, and  $m_m$  is the (mean) molecular mass.

When the speed ratio is high, the flow behaviour is dominated by the bulk velocity and is described as hypersonic. Contrastingly, when the speed ratio is small, the flow is dominated by the random thermal motion of the constituent particles and is described as hypersonic. The speed ratio determines the extent to which atmospheric particles can interact with surfaces parallel to or facing away from the oncoming flow direction and therefore their possible impact on the experienced aerodynamic forces. This can be particularly important when considering slender bodies that may have significant surface area parallel to the nominal flight direction. The speed ratio is generally observed to decrease with increasing altitude due to rising atmospheric temperature and as lighter atmospheric species become more abundant. The assumption of hypersonic flow is generally made for  $s > 5$ .

As indicated in Fig. 1, the atmospheric composition also varies significantly with altitude, and the transition between different regimes of atmospheric composition can critically affect GSI behaviour and the associated aerodynamic coefficients. However, despite the availability of numerous time-variant atmospheric models (e.g. NRLMSISE-00, JB2008, DTM2009 [15]) significant uncertainty remains regarding true atmospheric conditions (principally density, composition, and temperature) due to the complexity of the thermospheric/ionospheric system and lack of both spatially and temporally distributed measurements by both in situ and remote sensing methods [16, 17].

Above VLEO altitudes, the general reduction in density and AO concentration has been linked to a reduction in surface adsorption and therefore accommodation [18]. For

satellites at or above 500 km altitude, the transition from AO predominance to helium has been linked to drag modeling errors, attributed to assumptions in typical aerodynamic coefficient modelling and the reduction in molecular mass and surface adsorption of AO with altitude [19]. Analysis of satellites at 800–1000 km by Harrison and Swinerd [20, 21] has also indicated a reduction in surface accommodation and the presence of quasi-specular reflection behaviour.

The use of novel materials that have resistance to the effects of AO erosion and can reduce surface accommodation effects has been proposed as a means to reduce the drag experienced in orbit, even at lower altitudes, for example VLEO. The Satellite for Orbital Aerodynamics Research (SOAR) is a scientific 3U CubeSat that has been developed to provide validation data for extensive ground-based characterisation of GSI behaviour in VLEO and to perform the in situ test of candidate novel materials. SOAR was deployed on 14 June 2021 from the ISS into an initial orbit of 421 km  $\times$  415 km with inclination of 51.6°. This orbit will naturally decay to allow experiments to be performed at different altitudes in VLEO during the mission lifetime.

## 2 Modelling of gas–surface interactions and aerodynamic coefficients

A number of different models have been developed to mathematically express the exchange in energy and momentum between the oncoming particles in the atmospheric flow and the spacecraft surfaces with which they interact under different assumptions of the underlying physical processes and parameters of dependence. Such models can be used to calculate the dimensionless aerodynamic coefficients that relate the incident flow conditions to the forces that are experienced by a given surface.

In these models, the level of surface accommodation is typically expressed by accommodation coefficients that quantify the change in energy between the incident and re-emitted particles. The most basic of these, the thermal or energy accommodation coefficient  $\alpha_T$ , can be defined [8]:

$$\alpha_T = \frac{E_i - E_r}{E_i - E_s} = \frac{T_i - T_r}{T_i - T_w}, \quad (2)$$

where  $E_i$  and  $E_r$  are the kinetic energy of the particles incident on and re-emitted from the surface, respectively, and  $E_s$  is the energy that would be emitted from the surface (wall) if the particles had reached thermal equilibrium with the surface. Similarly,  $T_i$ ,  $T_r$ , and  $T_w$  are the temperatures associated with the kinetic energies previously defined.

Alternatively, two separate accommodation coefficients can be used to describe the normal  $\sigma_n$  and tangential  $\sigma_t$  momentum exchange occurring at the surface. These

accommodation coefficients can be defined analogously to Equation 2 using quantities of normal  $p$  and tangential momentum  $\tau$  respectively:

$$\sigma_n = \frac{p_i - p_r}{p_i - p_w}, \quad (3)$$

$$\sigma_t = \frac{\tau_i - \tau_r}{\tau_i} \quad (\tau_w = 0). \quad (4)$$

A number of GSI models have been developed that are commonly applied to the analysis of spacecraft aerodynamics:

1. Maxwell's model assumes a linear combination of the two extreme scattering behaviours. A fraction of the incoming particles (defined by an accommodation coefficient) are reflected specularly with no accommodation whilst the remaining fraction are re-emitted diffusely with complete thermal accommodation.
2. Schamberg's model [22] allows consideration of quasi-specular re-emission using a conical pattern with defined beam-width to define the reflected particle distribution. However, only hyperthermal flow conditions are assumed. This model is often used with Goodman's model for energy accommodation coefficient [23].
3. Sentman's model [24] is based on complete diffuse re-emission and accounts for the random thermal motion of the incoming particles. Moe et al. [25] introduced a thermal accommodation coefficient into this method, replacing the use of the reflected particle temperature to describe incomplete accommodation. This modification is also known as the Diffuse Reflection with Incomplete Accommodation (DRIA) model [10].
4. The Schaaf and Chambre model [26] utilises normal and tangential momentum accommodation coefficients to allow consideration of quasi-specular re-emission. Closed-form solutions for this model are given by Storch [27].
5. The Cercignani–Lampis–Lord (CLL) model [28] can reproduce diffuse and quasi-specular re-emission patterns using a normal energy accommodation coefficient and a tangential momentum accommodation coefficient. An analytical implementation of the CLL model based on the Schaaf and Chambre solutions

Further in-depth review and comparison of popular models for use in modelling of spacecraft aerodynamics are provided by Mostaza-Prieto et al. [6] and Livadiotti et al. [7].

Various GSI models have been used to study the aerodynamics of past and existing satellite missions and to infer suitable values of the accommodation coefficients that match the observed behaviour. Such analyses are critical for the development and improvement of models for atmospheric

density and thermospheric winds that are often dependent on the aerodynamic characterisation of such satellites themselves.

Investigation of the of the Proton 2, Ariel 2, Explorer 6 (paddlewheel-type) and S3-1 satellites by Moe et al. [8, 11] showed that below 200 km accommodation was almost complete and associated with diffuse re-emission behaviour. However, at higher altitudes and elliptical orbits associated with higher perigee velocity (and therefore kinetic energy) the accommodation was shown to decrease. Further analysis of a number of spherical satellites produced similar results whilst also indicating that accommodation falls more quickly with increasing altitude at solar minimum conditions due to the shrinking thermosphere and reduced AO abundance at higher altitudes during these periods [12, 29].

Pilinski et al. [30] subsequently developed a relationship between AO adsorption and energy accommodation for different altitudes based on the Langmuir isotherm, a function that relates the surface adsorption by a given gas species to its the partial pressure. This method was later modified [31] to incorporate a lower bound on the energy accommodation in the absence of AO based on Goodman's physical interaction model [32]. A similar approach developed by Walker et al. [28] uses the Langmuir isotherm to determine the fractional surface coverage by AO which is then applied as a weighting factor to combine drag coefficients calculated for clean and fully adsorbed surfaces. This fractional surface coverage approach also enables application to a wider range of GSI models (i.e. DRIA and CLL). Alternative adsorption models for fractional surface coverage have also been explored [33].

For very simple convex geometries (e.g. flat plates or spheres), closed-form analytical solutions of the GSI models can be used to calculate the overall aerodynamic forces and torques experienced by the given body exposed to the flow. However, for more complex geometries either panel methods or numerical approaches must be adopted. Flat-plate or panel methods operate by discretising a geometric model into a number of smaller elements (often triangular flat-plates) for which the individual aerodynamic contribution can be calculated using closed-form analytical GSI methods and summed together to generate the total aerodynamic coefficients for the body. However, these methods are unable to account for particle-particle interactions and multiple particle reflections from surfaces. Shadowing or shielding effects are also difficult to accurately account for due to the independent treatment of the surface elements, though ray-tracing approaches can be implemented, for example in ADBSat [34]. Panel methods are therefore only suitable for the analysis of generally convex geometries with simple external features, but due to their analytical basis can be executed very quickly for different orientations and environmental conditions [6]. Numerical approaches such

as test-particle Monte Carlo (TPMC) or direct-simulation Monte Carlo (DSMC) on the other hand use direct simulation of particles interactions with the spacecraft surfaces combined with statistical approaches to determine the aerodynamic coefficients for a given body. These methods can, therefore, account for more complex shadowing behaviour and the effect of multiple surface reflections, but at the expense of computational effort [35].

Hybridised or parametrised approaches can be used to reduce the computational burden of numerical-based approaches. Mehta et al. [35] implemented a Gaussian process based approach using DSMC results for the Grace spacecraft whilst also incorporating the fractional coverage method for surface accommodation. This response surface method has subsequently been implemented using TPMC to improve computational efficiency, and for a number of further satellite geometries [36, 37]. An alternative interpolation-based approach to drag coefficient modelling using DSMC simulations with high-fidelity geometric satellite models was implemented by March et al. [38]. Using results generated from this interpolation method in an analysis of neutral winds, updated energy accommodation coefficient values of 0.85 and 0.82 were proposed for the CHAMP and GOCE satellites respectively using the DRIA GSI model [39, 40].

For conventional materials the literature reviewed above, associated with on-orbit experiments and analysis of existing satellites, indicates that GSI behaviour in the AO-dominated environment of VLEO is dominated by significant accommodation and diffuse re-emission characteristics. More specifically, whilst  $\alpha_n$  is considered a variable parameter,  $\sigma_t$  is commonly assumed to be unity leading to diffuse re-emission behaviour [37, 41].

However, gas beam experiments suggest that characteristics such as the surface topology and orientation at the atomic scale may allow quasi-specular reflection properties in rarefied flows [42–44]. Recent experiments on the scattering properties of AO from different surfaces has demonstrated more specular reflection behaviour of silicon dioxide and highly orientated pyrolytic graphite (HOPG) [45], leading to investigation of further materials with AO erosion resistance for use in VLEO [46]. Study of nanofluidic channel flows, with a similar Knudsen number to that in VLEO, has also highlighted the existence of 2D materials exhibiting non-diffuse reflection behaviour [47]. Analysis of satellites at altitudes at and above the oxygen-helium transition regime has also suggested that tangential momentum accommodation may be significantly incomplete [19], suggesting that some conventional materials may demonstrate quasi-specular behaviour in orbit, albeit at altitudes above VLEO.

For consideration of surfaces or materials that may have AO erosion resistance and therefore the potential for a significant reduction in surface accommodation, representation

of a wide range of different re-emission qualities is therefore critical. The CLL model based on the closed-form Schaaaf and Chambre solutions will therefore be adopted in this work allowing a range of quasi-specular behaviour to be modelled. As there is no simple relationship between  $\sigma_n$  and  $\alpha_n$ , the species-specific fitted parameter approach developed by Walker et al [28] is used.

For the CLL model, when  $\alpha_n = 1$ , the incoming particles are completely accommodated to the surface and re-emitted in thermal equilibrium with the surface. Similarly, when  $\sigma_t = 1$  information of the tangential velocity of the incoming particles is lost and the re-emission will be diffuse. Contrastingly, when  $\alpha_n = \sigma_t = 0$ , the incoming particles will undergo elastic and specular reflection. For other values of  $\alpha_n$  and  $\sigma_t$  varying degrees of accommodation and quasi-specular behaviour can be modelled.

The drag coefficient ( $C_D$ ) and lift coefficient ( $C_L$ ) for a single-sided flat-plate with varying angle of incidence ( $\delta$ ) and varying values of the associated surface accommodation coefficient(s) are shown in Fig. 2 for the DRIA and CLL models. It should be noted that  $\alpha_n$  and  $\sigma_t$  have been varied together to reduce the parameter space for visualisation in Fig. 2. However, as noted above, for a given material or surface these two parameters may not necessarily be equal. The CLL model is able to express a much larger range of aerodynamic coefficients than presented here.

In Fig. 2a, the results for the DRIA model show that a reduction in  $\alpha$  results in an increase in drag coefficient even when the surface is oriented at shallow incidence angles. However, when quasi-specular reflection behaviour is considered using the CLL model a reduction in drag coefficient for reducing  $\alpha_n$  and  $\sigma_t$  is observed at shallow angles of incidence. However, when the surface is oriented towards the oncoming flow the reduction in  $\alpha_n$  and  $\sigma_t$  results in an increase in the drag coefficient. Unequal variations of  $\alpha_n$  and  $\sigma_t$  will result in varying behaviour of the aerodynamic coefficients and the surface angle at which a reduction in drag coefficient will be observed.

For both the DRIA and CLL models, an increase in the available lift coefficient is generally observed for reducing accommodation coefficient(s). The quasi-specular reflection behaviour of the CLL model provides a significantly greater magnitude of lift coefficient for most angles (except close to parallel to the flow) in comparison to the DRIA model. For reduced surface accommodation, the peak in the lift coefficient distribution is also slightly biased to orientations towards the normal inclination for the CLL model (30°–40°) compared to the DRIA model (~45°).

The variation in the aerodynamic coefficients is also shown to diminish with reducing accommodation and appears greatest close to the fully accommodated case. This is due to the expressions in the GSI models that relate the reflected particle energy or momentum with the respective

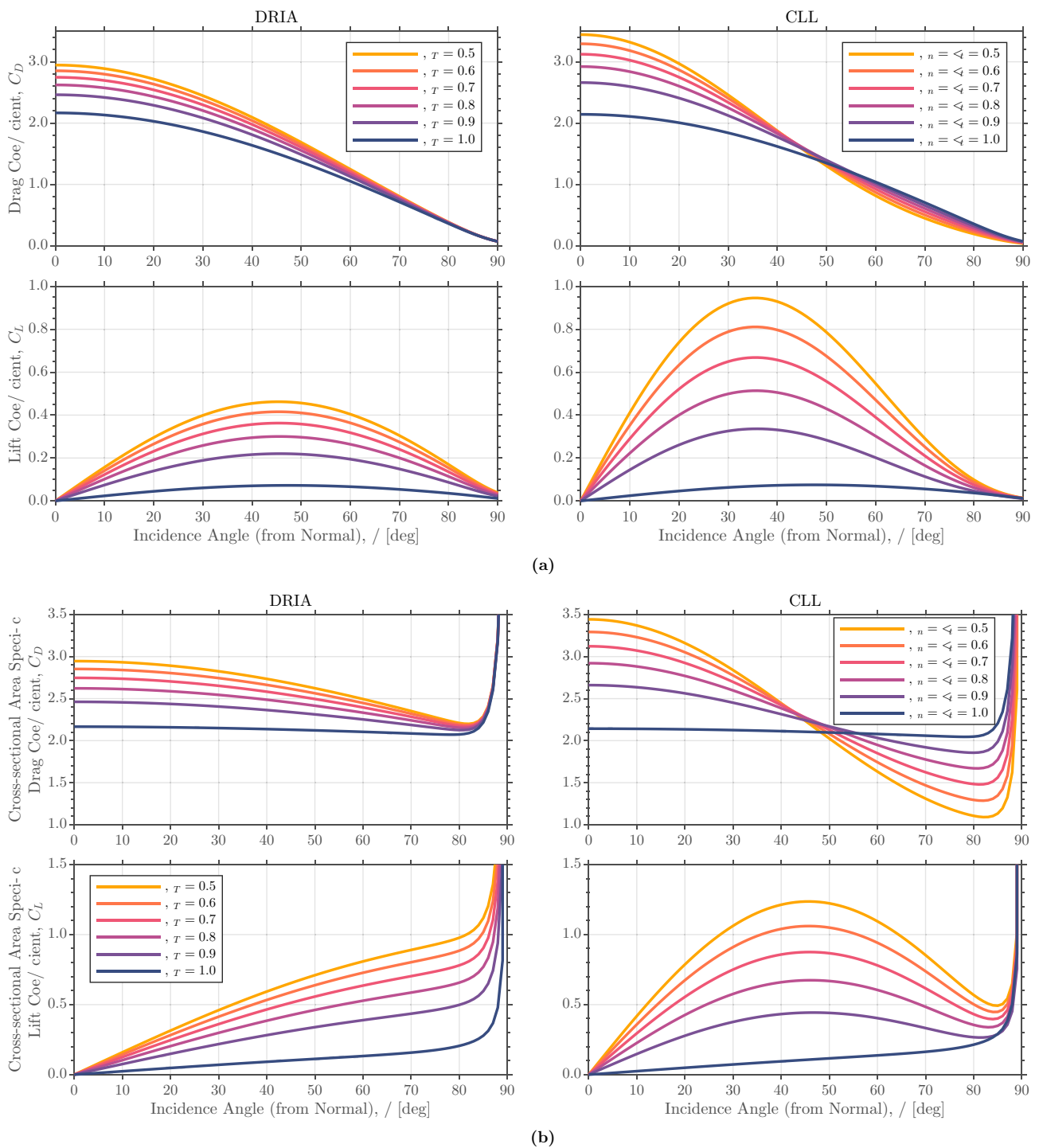


**Fig. 2** **a** Drag and lift coefficient for single-sided flat-plate with a reference area of 1 m<sup>2</sup>. **b** Drag and lift coefficient for a single-sided flat-plate referenced to the cross-sectional area at incidence angle  $\delta$ . Variation of the aerodynamic coefficients with incidence angle and input accommodation coefficient parameters for the DRIA and CLL

models. Atmospheric parameters (composition, temperature) have been calculated using the NRLSMSISE-00 model with medium solar activity conditions defined as per ISO 14222:2013 [5] at  $h = 300\text{km}$ ,  $T_w = 300\text{K}$ .

accommodation coefficient(s) and is physically due the high incident particle energy in comparison to that which a completely thermally accommodated particle would leave the surface with. For the CLL model, this effect is also more notable due to the assumption of quasi-specular scattering and therefore introduction of directionality of the reflected particle flux. As represented in Fig. 2a, this is principally due to the reduction in tangential momentum accommodation and demonstrated most clearly in the lift coefficient.

These results have been generated for medium solar activity conditions. At different solar activity conditions, the output force coefficients will change due to the variation in atmospheric composition and also the incident particle temperature at a given altitude (principally via the speed ratio). At increased solar activity conditions, the expanding atmosphere and, therefore, expectation for increased accommodation will generally result in a reduction in the force coefficients [13, 29]. Solar maximum conditions are associated with greater variations and uncertainty in the solar activity conditions and will therefore result in greater uncertainty in the aerodynamic coefficients during these periods [15]. A similar effect will also be presented due to atmospheric variations with latitude, shorter-term seasonal and diurnal cycles, and local-solar time [15, 17]. However, for VLEO altitudes where surface accommodation is typically assumed to be high, the sensitivity to these parameters is lower. The corresponding sensitivity of the aerodynamic coefficients to the wall temperature (here assumed static) is also low due to the relative magnitude compared to the incident particle temperature, i.e.  $T_w \ll T_i$  [28, 48].

In Fig. 2b the presented drag coefficient and lift coefficient are referenced to the cross-sectional (or projected) area with respect to the flow. This shows the effective variation of the aerodynamic coefficients independent of the change in cross-sectional area due to the orientation of the finite surface with respect to the flow. The rapid increase in the coefficients at incidence angles approaching  $90^\circ$  (i.e. parallel to the flow) should be recognised as a singularity resulting from the cosine function:  $\cos\left(\frac{\pi}{2}\right) = 0$ .

The results in Fig. 2b demonstrate clearly that for diffuse reflection characteristics a reduction in  $\alpha_r$  cannot enable a reduction in drag compared to a fully accommodated surface. However, under the assumption of quasi-specular reflection behaviour, variation of surface incidence can produce a reduction in drag, the magnitude of which is controlled by the specific combination of  $\alpha_n$  and  $\sigma_t$ .

This reduction of drag experienced in orbit is a critical challenge for satellites that operate in the VLEO environment. Contrastingly, the development of surfaces that can provide an increase the drag has application to the development of enhanced deorbit devices. An increase in the production of lift is also desirable for purposes of enhanced

aerodynamic control authority. However, to provide these desired aerodynamic characteristics, materials that can produce specular or quasi-specular reflection behaviour with reduced levels of energy accommodation are, therefore, needed. The development of such materials also has significance for the development of atmospheric intakes with greater efficiency [49]. These intakes are an important component of atmosphere-breathing electric propulsion (ABEP) systems that may be used to enable sustained drag compensation in VLEO [50].

### 3 The Satellite for Orbital Aerodynamics Research

The identification and characterisation of materials with enhanced aerodynamic properties has been a key focus of the DISCOVERER project that is working towards enabling satellites that can operate sustainably in VLEO [51, 52]. Critically, materials that are resistant to the adverse effects of AO adsorption and erosion may hold the promise of improvements to GSI performance in VLEO.

A ground-based experimental facility to perform comprehensive testing and characterisation of different candidate materials is currently being commissioned at The University of Manchester. The Rarefied Orbital Aerodynamics Research (ROAR) facility has been designed to reproduce the characteristic flux and energy of AO found in VLEO within an ultra-high vacuum chamber that reflects the rarefied nature of the flow in the orbital environment. The scattering pattern and energies of the incident and reflected AO beam from the different samples will be measured by a suite of sensors to enable the characterisation of the GSI properties [53, 54].

The Satellite for Orbital Aerodynamics Research (SOAR) has been designed to perform in situ characterisation of the aerodynamic performance of different materials at varying altitude and incidence angle in the VLEO environment [55], taking heritage from the previous  $\Delta$ Dsat mission concept [56]. The satellite will test novel 2D materials with promising orbital aerodynamic characteristics in-orbit and provide data to validate the ongoing experiments that will be conducted in the ROAR facility. SOAR will also demonstrate novel aerodynamic control manoeuvres [57, 58], provide measurements of the atmospheric flow in VLEO (density, composition, and velocity), and perform characterisation of the thermospheric wind vector [59].

SOAR, shown in Fig 3, is a 3U CubeSat with principal physical parameters reported in Table 1. The satellites features two payloads that work together to perform the envisaged experiments:

- An aerodynamics characterisation payload comprised of set of four individually steerable fins and associated



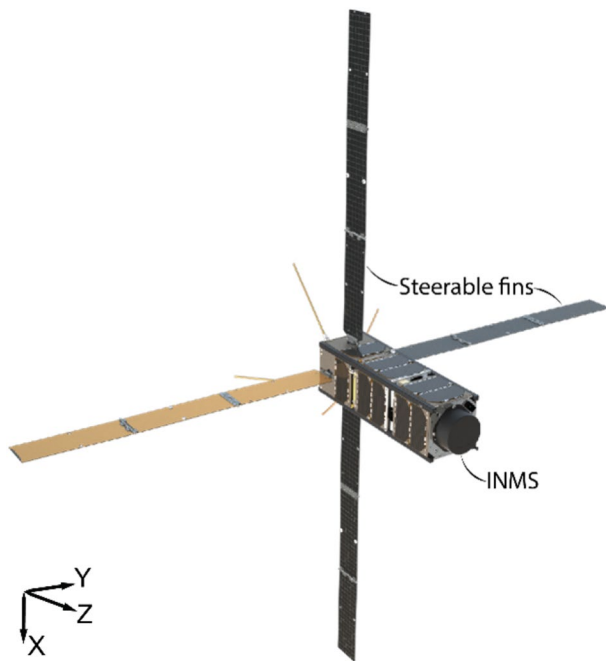


**Fig. 3** The Satellite for Orbital Aerodynamics Research (SOAR) with steerable fins in the minimum drag configuration. The spacecraft is nominally aligned with the z-axis into the oncoming flow direction

**Table 1** Geometric and system parameters of SOAR [55]

Property	Value
Mass (kg)	2.88
Length (in z-axis) ( $L_z$ ) (m)	0.366
Total surface area ( $A_T$ ) ( $m^2$ )	0.225
CoM (in z-axis from rear) (m)	0.161
Principal MoIs $\begin{Bmatrix} x \\ y \\ z \end{Bmatrix}$ ( $kg\ m^2$ )	$\begin{Bmatrix} 0.0392 \\ 0.0392 \\ 0.0288 \end{Bmatrix}$
Residual magnetic dipole (A m)	$18e-3$
RW max torque (N m)	$23e-6$
RW max ang momentum (N m s)	$1.2e-3$
RW spin axis MoI ( $kg\ m^2$ )	$694.5e-9$

control hardware. The panels comprising these fins are coated with four different experimental materials and arranged such that the opposing pairs of fins can be used to expose each material to the flow individually at varying angles of incidence. The fins are folded and stowed against the body of the satellite for launch and deployed after release into orbit.

- An atmospheric characterisation payload in the form of a forward-facing ion and neutral mass spectrometer (INMS) with time-of-flight capability that can measure

the density, composition, and velocity of the oncoming atmospheric flow.

The satellite also features a capable attitude determination and control system (ADCS) consisting of coarse and fine sun sensors (FSS), magnetometers, a state-of-the-art MEMS inertial measurement unit (IMU), magnetorquers, and a 3-axis reaction wheel assembly (RWA). A GPS receiver is also included to provide more precise orbital position/velocity information than is available from ground-based tracking and TLE information. A breakdown of the contributing components is provided in Fig. 4.

When the surfaces of the steerable fins are all aligned either parallel or perpendicular to satellite body (i.e. the z-body axis in Fig. 3), known as the minimum and maximum drag configurations respectively, naturally restoring aerodynamic torques will be generated if the satellite begins to point away from the direction of the oncoming flow. These configurations are therefore nominally aerostable and are the default configurations for the spacecraft. When other configurations of the steerable fins are adopted, additional aerodynamic forces and torques will be generated and will be used advantageously to perform both the desired material characterisation experiments and the aerodynamic control demonstrations.

On SOAR, four different materials have been selected to cover the steerable fin surfaces: sputter-coated gold, borosilicate glass, and two novel surface coatings (not identified herein for IP protection purposes). The gold and borosilicate glass surfaces are both resistant to AO erosion and are chemically stable in the VLEO environment. However, they exhibit significant differences in their AO recombination

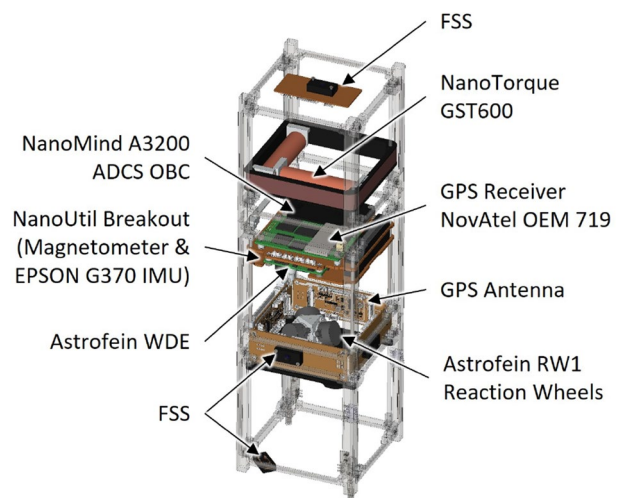


**Fig. 4** Components and configuration of the attitude determination and control system (ADCS) on SOAR

cross sections [60, 61] and have therefore been selected with the intention to provide breadth in GSI performance for previously characterised and well-known materials, i.e. from fully diffuse to more reflective respectively. The two “beyond graphene” 2D surface coating materials have been selected for their potential of improved GSI properties whilst also maintaining the necessary AO resistance.

The expected experimental uncertainty achievable by SOAR for materials demonstrating complete thermal accommodation and diffuse re-emission was previously reported in [55]. In this analysis, the lowest uncertainties for the drag coefficient determination were found at 300 km, whilst the determination of the lift coefficient was found to improve as the altitude was reduced to 200 km. However, these analyses may not be representative of the novel materials selected and present on the satellite. If these materials do provide lower energy accommodation or a greater degree of specular or quasi-specular re-emission, the forces and torques generated by the interaction of the coated surfaces would change, affecting the orbital and attitude response of the spacecraft.

Until the GSI characteristics of these materials are established from on-orbit investigation and laboratory-based experimentation their potential performance can only be speculated on. However, in order to explore the effect that such materials could have on the experimental performance of the SOAR mission, variation in the GSI models and associated accommodation coefficients can be applied in simulations and used to perform experimental uncertainty analyses, forming the focus of this paper.

#### 4 Experimental method for determining aerodynamic coefficients

Characterisation of the GSI performance of the different materials on SOAR will be performed by indirect estimation of the aerodynamic coefficients of the satellite with different configurations of the steerable fins. Measurements of the satellite position, velocity, attitude, and rotation rates will be performed in-orbit and methods of orbit and attitude determination will subsequently be performed to obtain best-fit estimates of the aerodynamic coefficients when the satellite is operated in different configurations. Environmental data measured by the INMS on-board the satellite will also be used to inform the orbit or attitude determination processes and reduce modelling uncertainties [55].

To ensure that only one material is nominally exposed to the flow at a time the steerable fins are operated in opposing pairs and as a result a maximum of four materials can be tested on SOAR. During the experiments, the opposing pairs of steerable fins can either be co-rotated or counter-rotated with respect to each other whilst exposing the same material to the flow. In these two configurations, the satellite

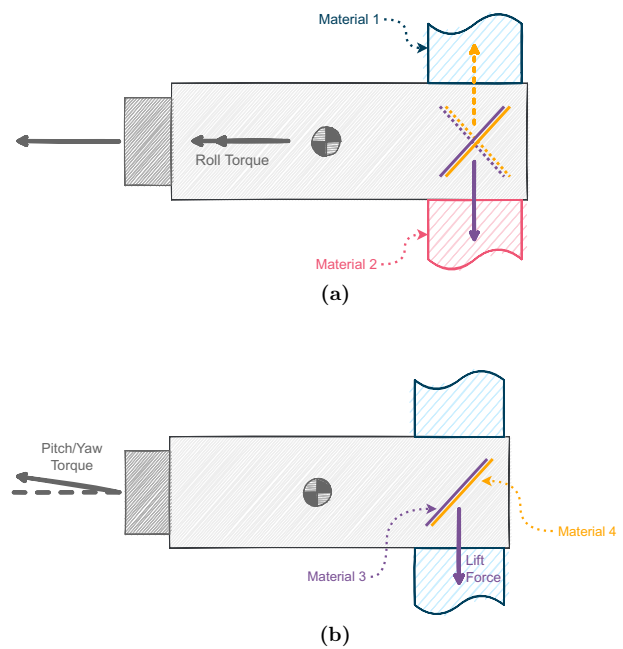


**Fig. 5** **a** Counter-rotated configuration **b** co-rotated configuration. Forces and torques generated by SOAR with different steerable fin configurations

will respond differently to the oncoming flow as a result of the variation in aerodynamic torques that are generated. The consequences of this on the experimental performance are explored in Sects. 5 and 6.

The INMS payload enables direct measurement of the in-situ density and composition during these experiments, reducing the uncertainty that is associated with the use of atmospheric models. However, to maintain the accuracy of the measurements, the aperture of the INMS instrument should nominally point closely towards the direction of the oncoming flow.

For counter-rotated configurations of two opposing steerable fins (Fig. 5a) and when the spacecraft is nominally pointed towards the oncoming flow, no net torques are generated in pitch or yaw. A rolling moment is, however, produced due to the opposing lift forces generated on the two exposed surfaces, which if left uncontrolled will result in roll of the spacecraft. If the spacecraft is disturbed from the flow pointing configuration, pitch and/or yaw torques will be produced. Coupling between motion in the pitch and yaw axes when the fins not in either the minimum or maximum drag mode may act to further disturb the attitude of the spacecraft from the flow-pointing direction.

For co-rotated configurations of two opposing steerable fins (Fig. 5b), the drag will similarly increase and a net pitch or yaw torque will be generated by the common incidence angle of rotated panels. This will cause the spacecraft to rotate and fly at an angle to the oncoming flow. The satellite

will also nominally oscillate about the new offset equilibrium attitude due to aerostability in this configuration.

In principle the counter-rotated configuration should ensure that the INMS instrument is pointed most precisely towards the oncoming flow direction and will be operated within its angular acceptance range. However, in either configuration, the effects of thermospheric winds and presence of other environmental torques (gravity gradient, solar radiation pressure and residual magnetic dipole interactions) will disturb the attitude of the spacecraft. Thus, during experiments for both counter-rotated and co-rotated steerable fin configurations the RWA will be used to selectively damp and control the motion of the spacecraft in different axes to provide the desired stability and pointing performance.

Practically, a maximum duration on operations with the fins in either a counter-rotated or co-rotated configuration will be imposed by the build-up of angular momentum and saturation of reaction wheels. This is a function of the atmospheric density, configuration and incidence angle of the steerable fins, and material GSI performance. The thermospheric wind, solar activity, and other external disturbance torques also contribute to the attitude stability and control performance. At lower altitudes the time-period over which spacecraft can be operated successfully may be significantly limited for some configurations, the impact of which will be investigated in Sects. 5 and 6.

This method, however, only strictly allows for the direct calculation of the composite aerodynamic force coefficients of the entire spacecraft in a given configuration rather than for an individual material. This is principally due to the aerodynamic contribution of the spacecraft body and interference between the body and the panels (i.e. shadowing and secondary particle interactions) that cannot be directly eliminated in the experimental analysis. As described by Virgili Llop & Roberts [56], a differential approach can be applied to calculate the ratio between aerodynamic coefficients for different combinations of material, incidence angle, and altitude. The relative measure of the aerodynamic performance between different materials or configurations can therefore be calculated whilst also avoiding biases and systematic errors, for example in the measurement of the atmospheric density.

#### 4.1 Orbit and attitude determination

Orbit and attitude determination methods will be used in ground-based post-processing to determine the aerodynamic coefficients from the experimentally gathered data. These methods utilise models to generate estimates for the contributing perturbing forces and torques. The in situ atmospheric density measured by the INMS can be used to reduce uncertainty and improve the aerodynamic force and torque model outputs. The resulting trajectory or attitude of the spacecraft

generated by propagation of these models can be compared to the orbital parameters or attitude measured by the GPS or ADCS, respectively.

Initial values of the drag or lift coefficients, possibly informed by ground-based experimental results if available, will be used to establish the aerodynamic coefficients corresponding to a given configuration of the steerable fins (and therefore exposed material) and initiate the orbit or attitude determination process. The iterative process of least-squares based differential correction will then provide the best-fit output aerodynamic coefficients to match the measured on-orbit data and the propagated trajectory or attitude.

The accuracy of this method, and therefore the returned aerodynamic coefficients, are dependent on both the accuracy and fidelity of the models that are used to perform the propagation and the uncertainty of the parameters measured on-orbit that are used as both inputs to these models and the orbit and attitude determination processes. Values for the expected performance of the sensors on SOAR are reported in Table 2. For the INMS, the basic instrument sensitivity can be determined by considering the uncertainty on the number density and combined with the expected reduction in acceptance given the pointing error with respect to the oncoming flow.

#### 4.2 Drag coefficient

Experiments to investigate the drag coefficient of the different materials can be performed using both counter-rotated and co-rotated configurations of the steerable fins and determining the overall drag coefficient of the spacecraft. In either configuration, the RWA will be used to stabilise the spacecraft attitude and maintain an approximately flow-pointing condition.

As the effect of the drag force accumulates over time to produce a variation to the orbital parameters, the drag coefficient of the spacecraft in a fixed experimental configuration can be determined using the least-squares orbit determination and free-parameter fitting method. With a fixed configuration of the steerable fins and a stabilised attitude, the

**Table 2** Expected SOAR sensor performance [55]

Instrument	Uncertainty
GPS position (m)	2.5 ( $1\sigma$ )
GPS velocity ( $\text{m s}^{-1}$ )	45e-3 ( $1\sigma$ )
ADCS angle (rad)	0.2e-3 ( $1\sigma$ )
ADCS angular velocity ( $\text{rad s}^{-1}$ )	25e-3 ( $1\sigma$ )
INMS number density ( $\text{cm}^{-3}$ )	$\sqrt{N} + 0.7$ ( $1\sigma$ )
INMS horizontal acceptance (rad)	0.279 (FWHM)
INMS vertical acceptance (rad)	0.035 (FWHM)
Steerable fin rotation angle (rad)	0.015 ( $1\sigma$ )

position and velocity vectors of the satellite can be measured over time using the GPS device and the in-situ atmospheric conditions using the INMS.

As the drag force results in a secular variation in the orbital parameters, these experiments can be performed even at the higher altitudes after deployment ( $\sim 400$  km) where the atmospheric density is lower, and the relative magnitude of the aerodynamic forces are small. However, at these higher altitudes, the experimental duration required to provide a discernible variation in the measured orbital parameters may be long and eventually limited by the power constraints of the platform when the different payloads, attitude actuators, and sensors are simultaneously operating.

As the satellite descends in altitude, the magnitude of the drag force will increase in comparison to the other external forces and the effect on the orbital parameters in a given period will become more significant. The experimental uncertainty would, therefore, be expected to generally decrease with altitude. However, as a result of the increasing magnitude of the disturbing aerodynamic torques, the maximum experimental duration will likely be constrained by the rate of saturation of the RWA in one or more axes.

The possible experimental duration at both the higher and lower altitudes may, therefore, not be sufficient to provide a good fit for the drag coefficient given the variation in the orbital parameters (i.e. the obtained signal to noise ratio). A trade between the ability for the spacecraft to operate in the experimental mode and the associated uncertainty on the output drag coefficient, therefore, exists. The optimal results are expected to be obtained between altitudes of approximately 350 km and 250 km [55].

### 4.3 Lift coefficient

The lift coefficients of the different experimental materials can be investigated through measurement of the rolling moment coefficient of the satellite. Counter-rotated configurations of the steerable fins will be adopted and the satellite will be allowed to rotate in the roll axis, whilst stabilisation is provided in the pitch and yaw axes by the RWA.

In addition to the intentionally generated aerodynamic torques, the satellite attitude will also be affected considerably by the other external perturbations. At higher altitudes, these other external torques are expected to be of a similar or greater magnitude than those generated by the aerodynamic interactions. As altitude reduces, the aerodynamic torques will increase in both relative and absolute magnitude and their effect on the satellite attitude will become dominant.

Using the on-board attitude sensors (combined using an unscented Kalman filter), the motion of the satellite during the lift coefficient experiments can be recorded alongside the orbit parameters and the properties of the oncoming flow as measured by the INMS. The method of least-squares

attitude determination with free-parameter fitting can be used to determine the rolling moment coefficient ( $C_l$ ) for the experimental configuration. The lift coefficient of the counter-rotated surfaces can subsequently be determined under the assumption that the two fin surfaces equally contribute to produce the rolling motion and that the remainder of the spacecraft does not produce any torques contributing to this motion.

In contrast to the drag coefficient experiments, the experimental uncertainty for the lift coefficient is expected to decrease as the altitude reduces. This is due to the increasing magnitude of the generated aerodynamic torques that will be clearly identifiable in the attitude measured by the ADCS, despite the reducing experimental period.

## 5 Attitude simulations

During the experimental operations co-rotated or counter-rotated configurations of the steerable fins will be utilised to expose the different materials to the oncoming flow, modifying the natural stability and attitude dynamics of the spacecraft. Stabilisation and control of the spacecraft against secular external disturbances will cause the build-up of the angular momentum in the RWA towards saturation and ultimately loss in control authority. For aerodynamic torques these effects are strongly linked to the dynamic pressure and will therefore increase with the density as the mission progresses and the satellite descends in altitude. The GSI performance of the surfaces of the steerable fins may also result in variations in the attitude dynamics of the spacecraft and therefore the experimental performance, particularly if the selected materials do demonstrate substantially different energy or momentum accommodation characteristics.

In the following simulations, the attitude behaviour of SOAR with different steerable fin and RWA control modes is considered for two GSI models and different input assumptions:

- The DRIA model with complete thermal accommodation ( $\alpha_T = 1.0$ ) representing conventional material performance.
- The CLL model with incomplete normal energy accommodation ( $\alpha_n = 0.9$ ) and tangential momentum accommodation ( $\sigma_t = 0.9$ ) representing a material with some quasi-specular reflection properties.

An altitude of 250 km has been selected as this was previously identified as a challenging case for the attitude control system whilst the steerable fins are configured to perform different experiments [55]. At higher altitudes the disturbing aerodynamic torques are smaller in magnitude and attitude control system is expected to be able to provide a

stable attitude over a longer period of time before saturation occurs. Commensurately, at lower altitudes the duration for which a stable attitude can be maintained in non-aerostable conditions is expected to decrease.

The response of SOAR under three-axis attitude control with one set of steerable fins counter-rotated at an angle of  $30^\circ$  is shown in Fig. 6. In both cases, a small offset of the attitude in yaw (with respect to the flow) initially appears as the Local-Vertical Local-Horizontal (LVLH) reference for the attitude control is not aligned directly with the oncoming flow due to atmospheric co-rotation. As a result of this misalignment, the aerodynamic torques, and the additional external disturbances, one or more of the wheels in the RWA are shown to reach saturation. This results in a loss of control actuation and the attitude eventually increases beyond the acceptance range of the INMS.

The accumulation of angular momentum and period before saturation and loss of control is much quicker for the case where the CLL model with incomplete accommodation is assumed. This is attributed to the increase of the lift coefficient associated with the GSI performance resulting in greater aerodynamic roll torques generated by the counter-rotated configuration and additional disturbing aerodynamic torques that are generated by the misalignments of the fins with the oncoming flow direction.

Corresponding results for a co-rotated steerable fin configuration are shown in Fig. 7. For both GSI models and associated assumptions, the period prior to RWA saturation and loss of attitude control is notably longer than in the counter-rotated configuration. This is principally a result

of the symmetry of the co-rotated configuration that yields some aerostable behaviour rather than the diverging roll torques and pitch-yaw coupling effects of the counter-rotated configuration. The difference in duration between the stabilised attitude behaviour of the two GSI models and associated inputs is however still notable.

In Figs. 6 and 7 it can be seen that prior to saturation of the RWA the attitude in pitch and yaw of the spacecraft is maintained within a small angular range ( $<5^\circ$ ) and therefore within the acceptance angle range of the INMS, enabling effective measurement of the in-situ density. However, if the duration over which the desired configuration of the steerable fins can be sustained prior to RWA saturation is shorter, an increase in the uncertainty of the drag coefficient determined using the orbit determination process is likely. This is investigated using statistical methods in Sect. 6.

Despite the expected disadvantage of the co-rotated configuration introducing an offset in the body attitude with respect to the flow (in yaw due to the rotation of the vertical fins in this case), the angle of rotation is small and comparable to that also seen for the counter-rotated configuration. This offset arises primarily due to the difference between the oncoming flow direction and the LVLH reference that is used by the ADCS. This is due to lack of knowledge of the true oncoming flow direction as a result of the thermospheric winds and to a lesser extent atmospheric co-rotation relative to the inclined orbit.

The location of the satellite with respect to the sun (i.e. eclipsed or not eclipsed) is also indicated in Figs. 6 and 7 using the shaded background and represents whether the

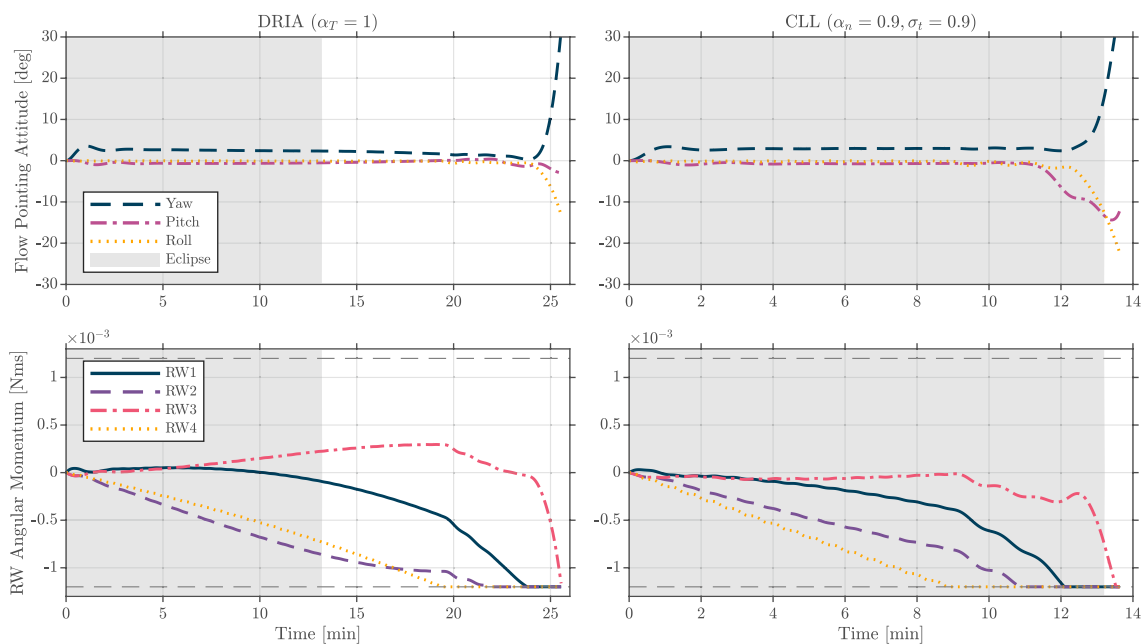


Fig. 6 Attitude response of SOAR at 250 km altitude with vertical steerable fins counter-rotated at  $30^\circ$  and three-axis reaction wheel control

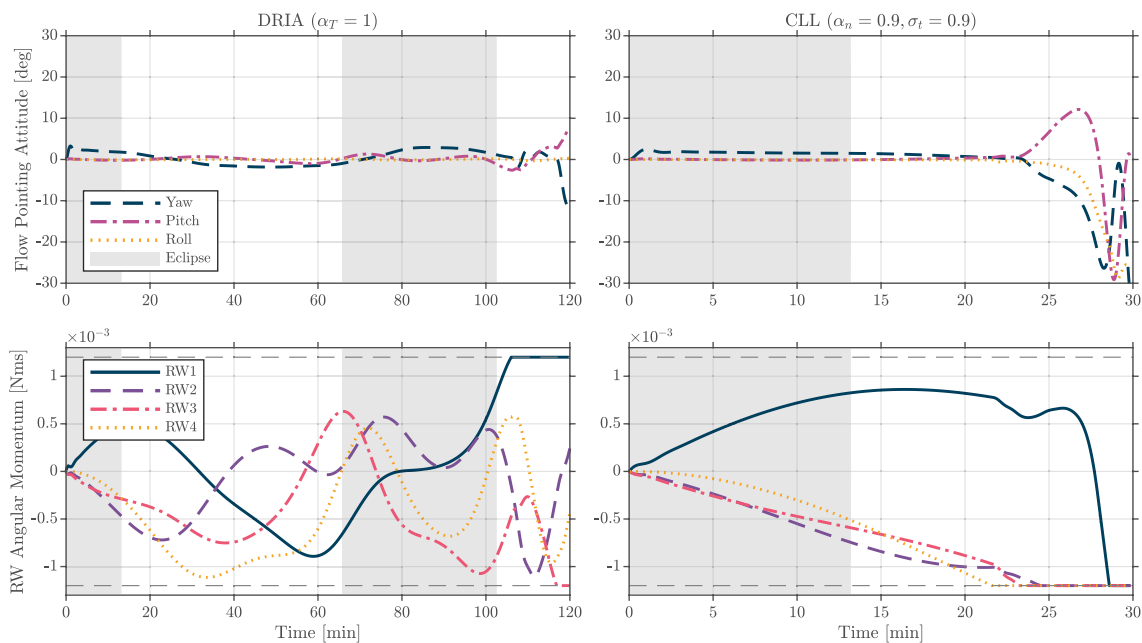


Fig. 7 Attitude response of SOAR at 250 km altitude with vertical steerable fins co-rotated at 30° and three-axis reaction wheel control

satellite is also under the influence of effects due to solar radiation pressure (SRP). The variation of the solar vector and interaction with the spacecraft surfaces means that the contribution of torques due to SRP may assist or disturb the spacecraft attitude control and stability at different times. However, at an altitude of 250 km, the torque due to SRP on SOAR is an order of magnitude less than the aerodynamic disturbances and is not therefore the dominant factor in the spacecraft attitude. Moreover, the attitude is further influenced by the other perturbing torques such as magnetic dipole interactions. Within the experimental analysis the effect of these perturbations is accounted for using models within the propagation and least-squares orbit/attitude determination method such that the impact of the aerodynamic forces and torques can be isolated.

The behaviour for a 30° counter-rotated configuration under two-axis control (pitch and yaw) is shown in Fig. 8. With the roll axis left uncontrolled, the torques generated by the two counter-rotated fins produce a couple (i.e. a moment with no net force) in the roll axis and the satellite will begin to rotate.

The rate at which the spacecraft angular velocity increases in the roll axis is faster for the case in which incomplete accommodation is assumed (using the CLL model). This is the expected result of the significant increase in the surface lift coefficient (see Fig. 2) and is clearly demonstrated by the time taken for a cumulative roll angle of 90° to be exceeded by the satellite (note the different time-scale of the x-axis for the two cases in Fig. 8). In both cases, the pitch and yaw axes are maintained close to the flow pointing direction, thus

enabling characterisation of the oncoming flow by the INMS instrument.

## 6 Experimental uncertainty with varying material performance

The experimental performance of SOAR for different assumed GSI properties of the test materials can be explored for different steerable fin configurations, incidence angles, and altitude. Orbit and attitude data generated by numerical propagation is used to simulate on-orbit data and then provided as input to the least-squares orbit/attitude determination method with free-parameter fitting that is used estimate the aerodynamic coefficients. Simulated sensor bias and noise is applied to the initial simulations to resemble the on-orbit sensor performance and therefore allow a measure of the expected experimental uncertainty [55].

For the initial orbital and attitude simulations, higher-fidelity perturbation models are utilised: Earth gravity (using EGM), third-body gravity, gravity gradient torques, SRP force and torques, aerodynamic force and torques, and residual magnetic dipole torques. For the SRP and aerodynamic models an interpolated database generated beforehand using the ADBSat panel method is used provide attitude dependent force and torque coefficient values for the SOAR geometry (with selected configuration of the steerable fins). The least-squares orbit and attitude determination processes are subsequently applied using the same propagation method. However, within this iterative process the aerodynamic force

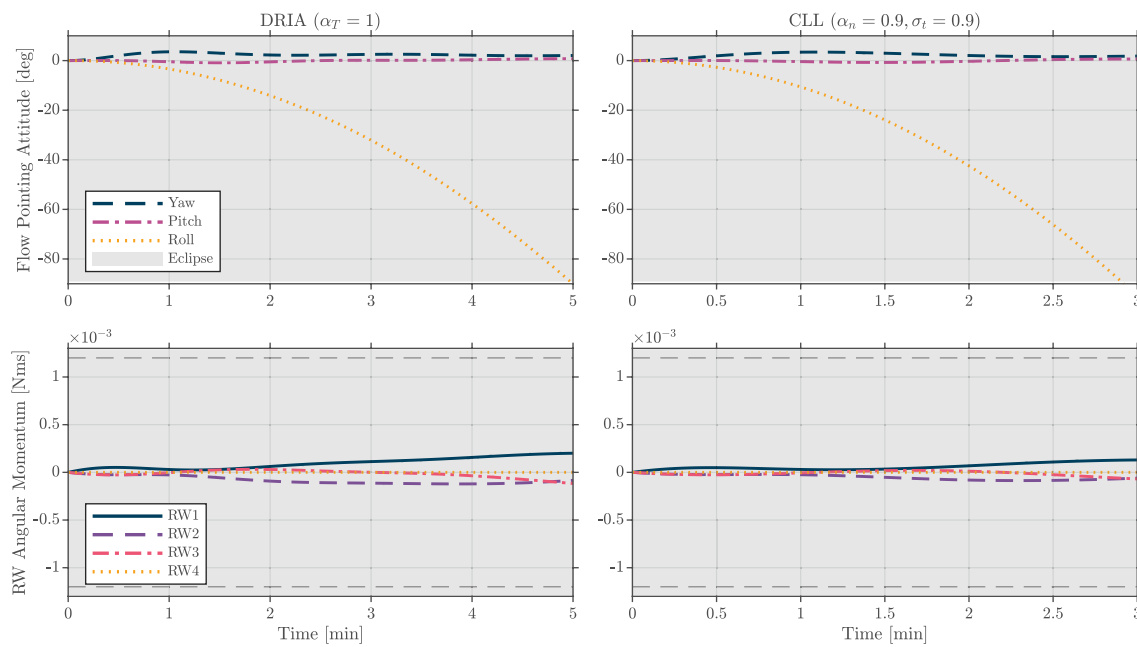


**Fig. 8** Attitude response of SOAR at 250 km altitude with vertical steerable fins counter-rotated at  $30^\circ$  and two-axis (pitch and yaw) reaction wheel control

and torque models are reduced to a simpler attitude-invariant methods to allow the free parameter fitting of the aerodynamic coefficients.

A Monte Carlo approach (using 50 runs) is been used for each case to consider the effect of variations in the initial orbit and attitude parameters in the absence of the in-flight data. The standard deviation of the returned aerodynamic coefficients, therefore, provides a measure of the expected uncertainty in the experimental and associated data-analysis method. An associated 95% confidence interval on the standard deviation is also included based on the number of Monte Carlo runs performed.

## 6.1 Drag coefficient

Figure 9 shows the mean fitted drag coefficient and associated standard deviation generated using least-squares orbit determination method and Monte Carlo approach for different assumed accommodation coefficient values (using the CLL model) with varying steerable fin configuration, incidence angle, and altitude. These figures express the expected experimental performance of the drag coefficient determination process.

Noting the varying scale on the y-axes, these figures show that for inclined steerable fins configurations (i.e. not at  $90^\circ$ ), decreasing the surface accommodation results in an increase in the experimental uncertainty. This is attributed to the greater lift force that is associated with lower surface accommodation coefficient and therefore an increase

in production of disturbing aerodynamic torques that must be compensated for by the ADCS. This effect is especially marked at low orbital altitude when the duration for which the experimental configuration can be effectively managed by the onboard attitude control actuators is very short. When the selected pair of steerable fins are deflected at  $90^\circ$  (nominally normal to the oncoming flow), the experimental uncertainty is much smaller for all accommodation coefficients. This is due to the aerostable nature of this configuration that reduces the attitude control requirements and allows a greater experimental duration.

For counter-rotated configurations (Fig. 9a) the experimental uncertainty is found to be generally smallest at 400 km in altitude. Comparatively, for co-rotated cases (Fig. 9b) the experimental uncertainty is found to be minimised at 300 km for each combination of the accommodation coefficients and incidence angle. Experiments performed with pairs of steerable fins oriented normal to the oncoming flow do not show the same trend and have the higher experimental uncertainty at 400 km altitude compared to 300 km and 200 km.

For cases with inclined steerable fins, both the counter-rotated and co-rotated configurations demonstrate sensitivity to the reduction in accommodation coefficient, resulting in significantly increased uncertainty. For the counter-rotated configuration, the standard deviation of cases with incomplete accommodation at 200 km altitude can exceed the magnitude of the drag coefficient, suggesting that a good estimation cannot be obtained. The co-rotated configuration

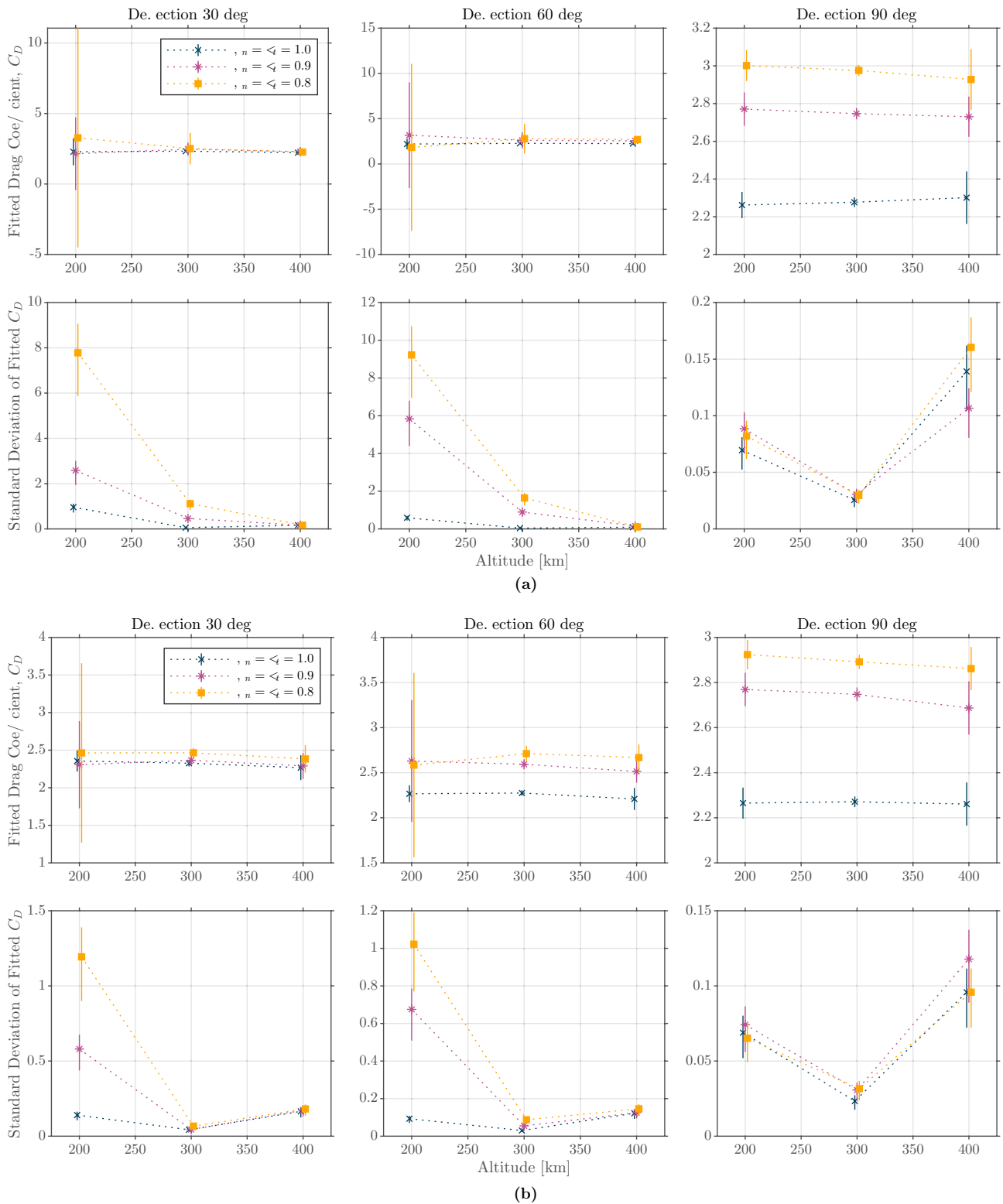


**Fig. 9** **a** Counter-rotated steerable fin configurations **b** co-rotated steerable fin configurations. Expected uncertainty of SOAR drag coefficient experiments with varying surface accommodation and altitude. Mean fitted drag coefficient (top) with error-bars representing

the associated standard deviation. Sample standard deviation (bottom) with error bars representing the 95% confidence interval. Data points have been shifted slightly in the  $x$ -axis to allow for visibility of overlapping error bars



shows a similar but smaller increase in experimental uncertainty for inclined surfaces at 200 km. In general, this suggests that the proposed experiments with inclined surfaces will be unable to provide clearly differentiable estimations of the drag coefficient, particularly at low orbital altitudes. However, at the higher orbital altitudes the experimental uncertainty is expected to decrease considerably and the variation in the drag coefficient as a result of material properties may be observed. Comparatively, when two opposing fins are rotated normal to the flow, the variation in drag coefficient due to different material properties should be more clearly visible.

### 6.2 Rolling moment coefficient

The corresponding experimental performance for varying surface accommodation in the rolling moment coefficient experiments is shown in Fig. 10. The experimental uncertainty is shown to be greater at higher altitudes and is attributed to the longer time taken for the satellite to roll through the requested 90° angle, due to the lower density and, therefore, lower magnitude of the aerodynamic roll torque. When this manoeuvre takes longer to perform the other perturbing torques are able to have a greater relative impact on the

satellite attitude, increasing the uncertainty in the returned coefficient.

Similarly to the results of the drag coefficient, the experimental uncertainty also increases with reducing accommodation coefficient. However, this uncertainty remains very small in comparison to the magnitude of the fitted rolling coefficient. As a result of the significant effect of incomplete accommodation on the lift coefficient (see Fig. 2), the standard deviation relative to the rolling moment coefficient magnitude is in fact improved for the cases  $\alpha_n = \sigma_t = 0.8$  and  $\alpha_n = \sigma_t = 0.9$  that remain below 5% and 7% respectively. In contrast, the standard deviation as a percentage of the absolute rolling moment coefficient for the case of complete accommodation is much higher, particularly at the 400 km altitude (10–25%).

These results suggest that if materials with some incomplete accommodation characteristics are indeed present on the steerable fin surfaces, the experimental uncertainty associated with the determination of the rolling moment coefficient will remain relatively low even at higher altitudes. Furthermore, given the magnitude of this uncertainty in comparison to the rolling moment coefficient, the variation between materials with different accommodation coefficients are likely to be clearly distinguishable from the experimental results using this method.

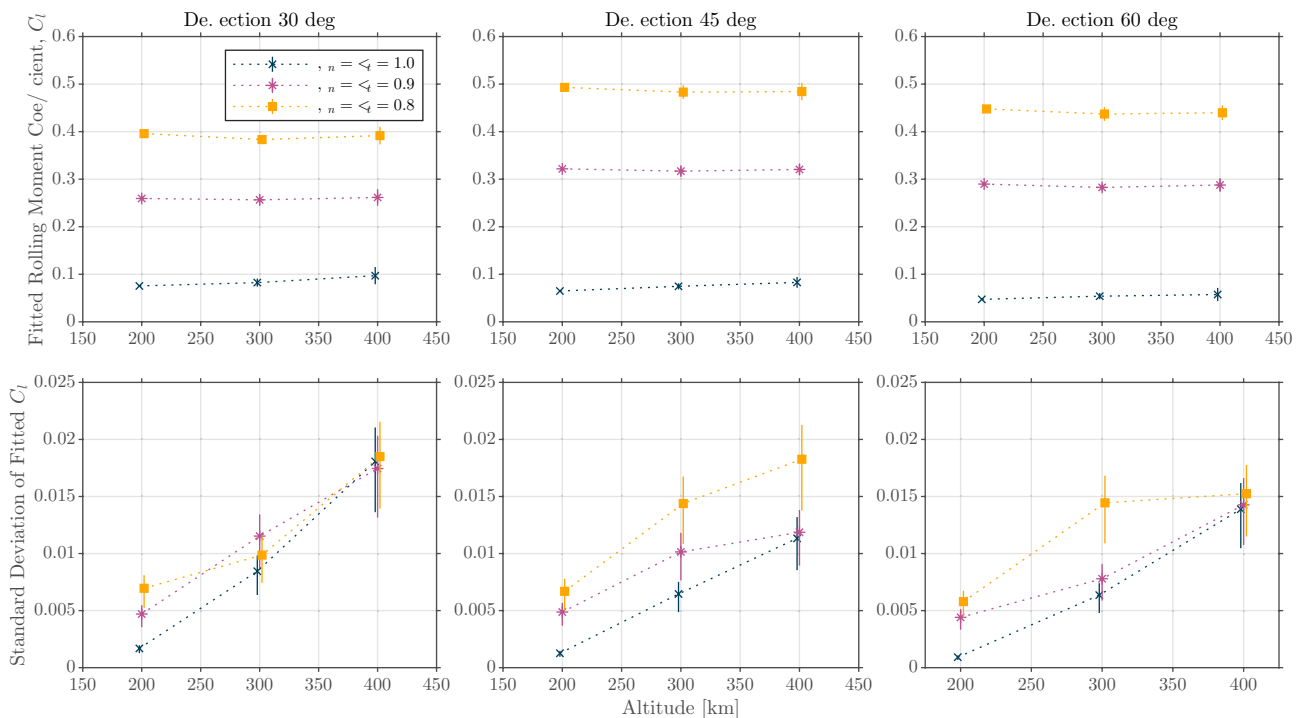


**Fig. 10** Expected uncertainty of SOAR rolling moment coefficient experiments with varying surface accommodation and altitude using counter-rotated steerable fin configurations. Mean fitted drag coefficient (top) with error bars representing the associated standard deviation.

tion. Sample standard deviation (bottom) with error bars representing the 95% confidence interval. Data points have been shifted slightly in the x-axis to allow for visibility of overlapping error bars

## 7 Conclusions and future work

The Satellite for Orbital Aerodynamics (SOAR) has been developed to perform novel testing of the aerodynamic coefficients of different materials in the rarefied VLEO environment and provide valuable in-situ data to support further systematic ground-based experimentation in the forthcoming Rarefied Orbital Aerodynamics Research (ROAR) facility at The University of Manchester. The aim of this work is to support the development of spacecraft that can operate sustainably at lower orbital altitudes with particular application to future commercial Earth observation and communications missions.

SOAR will also test two novel materials that have been identified for their potential to improve the aerodynamic performance of spacecraft in the rarefied flow environment of VLEO. Given the novelty and presently uncharacterised nature of these materials that will be tested on the satellite, uncertainty in their aerodynamic performance exists. In this paper, the experimental performance of SOAR has been analysed for different assumed GSI model characteristics and accommodation coefficient values. The performance of the experiments to determine the drag coefficient of the satellite were found to generally deteriorate with reducing surface accommodation and at very low altitudes (i.e. from 300 to 200 km). Co-rotated configurations of the steerable fins were comparatively shown to provide improved experimental performance. However, the most likely configuration to allow a clear differentiation of different material performance from the drag coefficient is found for pairs of opposing steerable fins rotated normal to the oncoming flow.

In contrast, the performance of the experiments to determine the satellite rolling moment coefficient (associated with the material lift coefficient) was found to be robust against variations in the surface accommodation whilst also improving as the orbital altitude reduces. As a result of this low uncertainty, these experiments are also expected to allow for differentiation of materials with different GSI properties or accommodation coefficients.

Future work will seek to connect the spacecraft aerodynamic coefficients, determined using the method presented in this paper, with the specific material properties of the steerable fin surfaces. The application of different GSI models and associated sets of accommodation coefficients will be considered to provide the best fit to the observed on-orbit behaviour. Subsequent direct characterisation of corresponding material samples from the ROAR facility will be used to provide supporting evidence of the material performance.

As a result of the performed analyses, a number of recommendations can be proposed to improve the

aerodynamic coefficient estimation method for SOAR. Development and implementation of improved perturbation models and characterisation of the satellite (e.g. SRP force and torque coefficients and the magnetic dipole) would contribute to reducing the uncertainties associated with the least-squares orbit determination method employed, and will be considered in future work. Improvements to the attitude control capabilities of the spacecraft, particularly with regards to the reaction wheel saturation limits, would also help to improve the experimental performance at lower altitudes by increasing the possible experimental duration. However, such improvements to the platform are limited due to the constrained nature of the 3U CubeSat form.

A number of further improvements may also be considered for future missions. Reduction in the uncertainty of the parameters measured in-orbit, namely the spacecraft position, velocity and, attitude, the atmospheric density, and the oncoming flow vector would help to increase the experimental sensitivity. This would principally require the use of additional or alternative sensors (e.g. use of a star-tracker for attitude determination) and improvements to the flow characterisation instrumentation. Additional on-orbit measurements, for example the direct measurement of accelerations and surface temperatures could help to improve the experimental performance. Finally, the ability to actively determine the oncoming flow direction to use this as the reference direction for attitude control would be advantageous in reducing the errors due to misalignment with the flow. However, such improvements are likely out of scope for a CubeSat-class mission.

SOAR was deployed into a 421 km  $\times$  415 km orbit with inclination of 51.6° in June 2021. This orbit will naturally decay as the spacecraft has no on-board propulsion, allowing access to different altitudes over the satellite lifetime. The presented results will be used to plan and schedule the experiments that will be performed by the spacecraft as it descends in orbital altitude to make best use of the limited lifetime and maximise the scientific return of the mission.

**Acknowledgements** This project has received funding from the European Union's Horizon 2020 research and innovation programme under grant agreement No 737183. This publication reflects only the view of the authors. The European Commission is not responsible for any use that may be made of the information it contains.

Members of the DISCOVERER Project:

The University of Manchester, Oxford Road, Manchester, M13 9PL, UK: N.H. Crisp, P.C.E. Roberts, A. Macario Rojas, V.T.A. Oiko, S. Edmondson, S.J. Haigh, B.E.A. Holmes, S. Livadiotti, L.A. Sinpetru.

GomSpace A/S, Langagervej 6, 9220 Aalborg East, Denmark: S. Christensen, V. Hanessian, M. Bisgaard, T.K. Jensen. Elecnor Deimos Satellite Systems, Calle Francia 9, 13500 Puertollano, Spain: V. Sullioti-Linner.

Institute of Space Systems (IRS), University of Stuttgart, Pfaffenwaldring 29, 70569 Stuttgart, Germany: Y.-A. Chan, S. Fasoulas, G.H. Herdrich, F. Romano, C. Traub.

UPC-BarcelonaTECH, Colom 11, TR5, 08222 Terrassa, Spain: D. García-Almiñana, M. García-Berenguer, S. Rodríguez-Donaire, M. Sureda.

Mullard Space Science Laboratory, University College London, Holmbury St. Mary, Dorking, Surrey RH5 6NT, UK: D. Kataria, S. Reddy.

Euroconsult, 86 Boulevard de Sébastopol, Paris, France: B. Belkouchi, A. Conte, S. Seminari, R. Villain.

**Author Contributions** NHC and PCER developed the experimental method and analysed the results. NHC performed the simulations, produced the results, and wrote the manuscript. PCER, VH, VS-L, GHH, DG-A, DK, and SS reviewed, provided feedback and approved the manuscript.

**Open Access** This article is licensed under a Creative Commons Attribution 4.0 International License, which permits use, sharing, adaptation, distribution and reproduction in any medium or format, as long as you give appropriate credit to the original author(s) and the source, provide a link to the Creative Commons licence, and indicate if changes were made. The images or other third party material in this article are included in the article's Creative Commons licence, unless indicated otherwise in a credit line to the material. If material is not included in the article's Creative Commons licence and your intended use is not permitted by statutory regulation or exceeds the permitted use, you will need to obtain permission directly from the copyright holder. To view a copy of this licence, visit <http://creativecommons.org/licenses/by/4.0/>.

## References

- Crisp, N.H., Roberts, P.C.E., Livadiotti, Sabrina, Oiko, V.T.A., Edmondson, S., Haigh, S.J., Huyton, Claire, Sinpetru, L.A., Smith, K.L., Worrall, S.D., Becedas, Jonathan, Domínguez, R.M., González, D., Hanessian, V., Mølgaard, A., Nielsen, J., Bisgaard, M., Chan, Y.-A., Fasoulas, S., Herdrich, G.H., Romano, F., Traub, C., García-Almiñana, D., Rodríguez-Donaire, S., Sureda, M., Kataria, D., Outlaw, R., Belkouchi, B., Conte, A., Perez, J.S., Villain, R., Heißeher, B., Schwalber, A.: The benefits of very low earth orbit for earth observation missions. *Prog. Aerosp. Sci.* **117**, 100619 (2020). <https://doi.org/10.1016/j.paerosci.2020.100619>(ISSN 03760421)
- Gavish, B., Kalvenes, J.: The impact of satellite altitude on the performance of LEOS based communication systems. *Wirel. Netw.* **4**(2), 119–213 (1998). <https://doi.org/10.1023/A:1019151905814>. ((ISSN 10220038))
- Walsh, J., Berthoud, L., Allen, C.: Drag reduction through shape optimisation for satellites in very low earth orbit. *Acta Astron.* **179**, 105–121 (2021). <https://doi.org/10.1016/j.actaastro.2020.09.018>. ((ISSN 00945765))
- Picone, J.M., Hedin, A.E., Drob, D.P., Aikin, A.C.: NRLM-SISE-00 empirical model of the atmosphere: statistical comparisons and scientific issues. *J. Geophys. Res.* **107**(A12), 1 (2002). <https://doi.org/10.1029/2002JA009430>. ((ISSN 0148-0227))
- ISO/TC 20/SC 14 Space systems and operations: ISO 14222:2013 Space environment (natural and artificial)—earth upper atmosphere. Standard, International Organisation for Standardization, Geneva, Switzerland (2013)
- Mostaza-Prieto, D., Graziano, B.P., Roberts, P.C.E.: Spacecraft drag modelling. *Prog. Aerosp. Sci.* **64**, 56–65 (2014). <https://doi.org/10.1016/j.paerosci.2013.09.001>. ((ISSN 03760421))
- Livadiotti, S., Crisp, N.H., Roberts, P.C.E., Worrall, S.D., Oiko, V.T.A., Edmondson, S., Haigh, S.J., Huyton, C., Smith, K.L., Sinpetru, L.A., Holmes, B.E.A., Becedas, J., Domínguez, R.M., Cañas, V., Christensen, S., Mølgaard, A., Nielsen, J., Bisgaard, M., Chan, Y.-A., Herdrich, G.H., Romano, F., Fasoulas, S., Traub, C., García-Almiñana, D., Rodríguez-Donaire, S., Sureda, M., Kataria, D., Belkouchi, B., Conte, A., Santiago Perez, J., Villain, R., Outlaw, R.: A review of gas-surface interaction models for orbital aerodynamics applications. *Prog. Aerosp. Sci.* **119**, 100675 (2020). <https://doi.org/10.1016/j.paerosci.2020.100675>. <https://linkinghub.elsevier.com/retrieve/pii/S0376042120300877>(ISSN 03760421)
- Moe, K., Moe, M.M., Wallace, S.D.: Improved satellite drag coefficient calculations from orbital measurements of energy accommodation. *J. Spacecr. Rockets* **35**(3), 266–272, (1998). <http://arc.aiaa.org/doi/10.2514/2.3350>(ISSN 0022-4650)
- Bowman, B.R., Moe, K.: Drag coefficient variability at 175–500 km from the orbit decay analyses of spheres. In: AAS/AIAA Astrodynamics Specialists Conference, pp. 1–20, Lake Tahoe, CA (2005). American Astronautical Society (AAS)
- Sutton, E.K.: Normalized force coefficients for satellites with elongated shapes. *J. Spacecr. Rockets* **46**(1), 112–116 (2009). <https://doi.org/10.2514/1.40940>. ((ISSN 0022-4650))
- Moe, M.M., Wallace, S.D., Moe, K.: Refinements in determining satellite drag coefficients—method for resolving density discrepancies. *J. Guid. Control Dyn.* **16**(3), 441–445 (1993). <https://arc.aiaa.org/doi/10.2514/3.21029>(ISSN 0731-5090)
- Moe, K., Bowman, B.R.: The effects of surface composition and treatment on drag coefficient of spherical satellites. In: AAS/AIAA Astrodynamics Specialists Conference, Lake Tahoe, CA, pp. 1–16 (2005). American Astronautical Society (AAS). ISBN 087703527X
- Doornbos, E.: Thermospheric Density and Wind Determination from Satellite Dynamics. Springer Theses. Springer, Berlin (2012). <https://doi.org/10.1007/978-3-642-25129-0>(978-3-642-25128-3)
- Gregory, J.C., Peters, P.N.: A measurement of the angular distribution of 5 eV atomic oxygen scattered off a solid surface in earth orbit. *Rarefied Gas Dyn.* **15**(1) (1987)
- Vallado, D.A., Finkleman, D.: A critical assessment of satellite drag and atmospheric density modeling. *Acta Astronaut.* **95**(1), 141–165 (2014). <https://doi.org/10.1016/j.actaastro.2013.10.005>. ((ISSN 00945765))
- Emmert, J.T.: Thermospheric mass density: a review. *Adv. Space Res.* **56**(5), 773–824 (2015). <https://doi.org/10.1016/j.asr.2015.05.038>. ((ISSN 18791948))
- Palmroth, M., Grandin, M., Sarris, T., Doornbos, E., Tourgaidis, S., Aikio, A., Buchert, S., Ciliverd, M.A., Dandouras, I., Heelis, R., Hoffmann, A., Ivchenko, N., Kervalishvili, G., Knudsen, D.J., Kotova, A., Liu, H.-L., Malaspina, D.M., March, G., Marchaudon, A., Marghitu, O., Matsuo, T., Miloch, W.J., Moretto-Jørgensen, T., Mpaloukidis, D., Olsen, N., Papadakis, K., Pfaff, R., Pirnaris, P., Siemes, C., Stolle, C., Suni, J., van den IJssel, J., Verronen, P.T., Visser, P., Yamauchi, M.: Lower-thermosphere-ionosphere (LTI) quantities: current status of measuring techniques and models. *Annales Geophysicae* **39**(1), 189–237 (2021). <https://doi.org/10.5194/angeo-39-189-2021>(ISSN 1432-0576)
- Moe, K., Moe, M.M.: Gas-surface interactions and satellite drag coefficients. *Planet. Space Sci.* **53**(8), 793–801 (2005). <https://doi.org/10.1016/j.pss.2005.03.005>. ((ISSN 00320633))
- Bernstein, V., Pilinski, M., Knipp, D.: Evidence for drag coefficient modeling errors near and above the oxygen-to-helium transition. *J. Spacecr. Rockets* **57**(6), 1246–1263 (2020). <https://doi.org/10.2514/1.A34740>. ((ISSN 0022-4650))
- Harrison, I.K., Swinerd, G.G.: Analysis of satellite laser ranging data to investigate satellite aerodynamics. *Planet. Space Sci.* **43**(8), 1023–1033 (1995). [https://doi.org/10.1016/0032-0633\(95\)00010-3](https://doi.org/10.1016/0032-0633(95)00010-3)

21. Harrison, I.K., Swinerd, G.G.: A free molecule aerodynamic investigation using multiple satellite analysis. *Planet. Space Sci.* **44**(2), 171–180 (1996). [https://doi.org/10.1016/0032-0633\(95\)00077-1](https://doi.org/10.1016/0032-0633(95)00077-1). ((ISSN 00320633))
22. Schamberg, R.: A New Analytic Representation of Surface Interaction for Hypothermal Free Molecule Flow with Applications to Neutral-particle Drag Estimates of Satellites. Rand Corporation, Research Memorandum (1959)
23. Goodman, F.O., Wachman, H.Y.: Formula for thermal accommodation coefficients. *J. Chem. Phys.* **46**(6), 2376–2386 (1967). <https://doi.org/10.1063/1.1841046>. ((ISSN 0021-9606))
24. Sentman, L.H.: Free molecule flow theory and its application to the determination of aerodynamic forces. Lockheed Missiles & Space Company, Sunnyvale, CA, Technical report (1961)
25. Moe, K., Moe, M.M., Rice, C.J.: Simultaneous analysis of multi-instrument satellite measurements of atmospheric density. *J. Spacecr. Rockets* **41**(5), 849–853 (2004). <https://doi.org/10.2514/1.2090>. ((ISSN 0022-4650))
26. Schaaf, S.A., Chambre, P.L.: Flow of rarefied gases. In: *Fundamental of Gas Dynamics*, volume III, chapter Section H, pp. 687–739. Princeton University Press, Princeton (1958) (ISBN 0691625700)
27. Storch, J.A.: Aerodynamic Disturbances on Spacecraft in Free-Molecular Flow. Tr-2003(3397)-1, The Aerospace Corporation, El Segundo, CA (2002)
28. Walker, A.C., Mehta, P.M., Koller, J.: Drag coefficient model using the Cercignani-Lampis-Lord gas-surface interaction model. *J. Spacecr. Rockets* **51**(5), 1544–1563 (2014). <https://doi.org/10.2514/1.A32677>. ((ISSN 0022-4650))
29. Pardini, C., Anselmo, L., Moe, K., Moe, M.M.: Drag and energy accommodation coefficients during sunspot maximum. *Adv. Space Res.* **45**(5), 638–650 (2010). <https://doi.org/10.1016/j.asr.2009.08.034>. ((ISSN 02731177))
30. Pilinski, M.D., Argrow, B.M., Palo, S.E.: Semiempirical model for satellite energy-accommodation coefficients. *J. Spacecr. Rockets* **47**(6), 951–956 (2010). <https://doi.org/10.2514/1.49330>. ((ISSN 0022-4650))
31. Pilinski, M.D., Argrow, B.M., Palo, S.E., Bowman, B.R.: Semi-empirical satellite accommodation model for spherical and randomly tumbling objects. *J. Spacecr. Rockets* **50**(3), 556–571 (2013). <https://doi.org/10.2514/1.A32348>. ((ISSN 0022-4650))
32. Goodman, F.O.: Three-dimensional hard spheres theory of scattering of gas atoms from a solid surface I. Limit of large incident speed. *Surf. Sci.* **7**, 391 (1967). ((ISSN 00396028))
33. Walker, A.C., Mehta, P.M., Koller, J.: The effect of different adsorption models on satellite drag coefficients. *Adv. Astronaut. Sci.* **150**, 675–686 (2014b). ((ISSN 00653438))
34. Sinpetru, L.A., Crisp, N.H., Mostaza-Prieto, D., Livadiotti, S., Roberts, P.C.E.: ADBSat: Methodology of a novel panel method tool for aerodynamic analysis of satellites. *Comput. Phys. Commun.* (2022). (accepted for publication)
35. Mehta, P.M., McLaughlin, C.A., Sutton, E.K.: Drag coefficient modeling for grace using Direct Simulation Monte Carlo. *Adv. Space Res.* (2013). <https://doi.org/10.1016/j.asr.2013.08.033>. ((ISSN 02731177))
36. Mehta, P.M., Walker, A.C., Lawrence, E., Linares, R., Higdon, D., Koller, J.: Modeling satellite drag coefficients with response surfaces. *Adv. Space Res.* **54**(8), 1590–1607 (2014). <https://doi.org/10.1016/j.asr.2014.06.033>. ((ISSN 18791948))
37. Mehta, P.M., Walker, A.C., Sutton, E.K., Godinez, H.C.: New density estimates derived using accelerometers on board the CHAMP and GRACE satellites. *Space Weather* **15**(4), 558–576 (2017). <https://doi.org/10.1002/2016SW001562>. ((ISSN 15427390))
38. March, G., Doornbos, E.N., Visser, P.N.A.M.: High-fidelity geometry models for improving the consistency of CHAMP, GRACE, GOCE and Swarm thermospheric density data sets. *Adv. Space Res.* **63**(1), 213–238 (2019). <https://doi.org/10.1016/j.asr.2018.07.009>. ((ISSN 02731177))
39. March, G., Visser, T., Visser, P.N.A.M., Doornbos, E.N.: CHAMP and GOCE thermospheric wind characterization with improved gas-surface interactions modelling. *Adv. Space Res.* **64**(6), 1225–1242 (2019b). <https://doi.org/10.1016/j.asr.2019.06.023>. ((ISSN 18791948))
40. March, G., van den IJssel, J., Siemes, C., Visser, P.N.A.M., Doornbos, E.N., Pilinski, M.: Gas-surface interactions modelling influence on satellite aerodynamics and thermosphere mass density. *J. Space Weather Space Clim.* **11**, 54 (2021). <https://doi.org/10.1051/swsc/2021035> (ISSN 2115-7251)
41. Sazhin, O.V., Borisov, S.F., Sharipov, F.: Accommodation coefficient of tangential momentum on atomically clean and contaminated surfaces. *J. Vac. Sci. Technol. A Vac. Surf. Films* **19**(5), 2499–2503 (2001). <https://doi.org/10.1116/1.1388622>. ((ISSN 0734-2101))
42. West, L.A., Somorjai, G.A.: Effects of surface disorder, various surface structures of chemisorbed gases and carbon on helium atomic beam scattering from the (100) surface of platinum. *J. Chem. Phys.* **54**(7), 2864–2873 (1971). <https://doi.org/10.1063/1.1675266>. ((ISSN 0021-9606))
43. Bernasek, S.L., Siekhaus, W.J., Somorjai, G.A.: Molecular-beam study of hydrogen-deuterium exchange on low- and high-Miller-Index platinum single-crystal surfaces. *Phys. Rev. Lett.* **30**(24), 1202–1204 (1973). <https://doi.org/10.1103/PhysRevLett.30.1202>. ((ISSN 0031-9007))
44. Sau, R., Merrill, R.P.: The scattering of hydrogen, deuterium, and the rare gases from silver (111) single crystals. *Surf. Sci.* **34**(2), 268–288 (1973). [https://doi.org/10.1016/0039-6028\(73\)90119-2](https://doi.org/10.1016/0039-6028(73)90119-2). ((ISSN 00396028))
45. Murray, V.J., Pilinski, M.D., Smoll, E.J., Qian, M., Minton, T.K., Madzunkov, S.M., Darrach, M.R.: Gas-surface scattering dynamics applied to concentration of gases for mass spectrometry in tenuous atmospheres. *J. Phys. Chem. C* **121**(14), 7903–7922 (2017). <https://doi.org/10.1021/acs.jpcc.7b00456>. ((ISSN 1932-7447))
46. Minton, T.K., Schwartzentruber, T.E., Xu, C.: On the utility of coated POSS-polyimides for vehicles in very low earth orbit. *ACS Appl. Mater. Interfaces* **13**(43), 51673–51684 (2021). <https://doi.org/10.1021/acsami.1c14196>. ((ISSN 1944-8244))
47. Keerthi, A., Geim, A.K., Janardanan, A., Rooney, A.P., Esfandiari, A., Hu, S., Dar, S.A., Grigorieva, I.V., Haigh, S.J., Wang, F.C., Radha, B.: Ballistic molecular transport through two-dimensional channels. *Nature* **558**(7710), 420–424 (2018). <https://doi.org/10.1038/s41586-018-0203-2>. ((ISSN 0028-0836))
48. Pilinski, M.D., Argrow, B.M., Palo, S.E.: Drag coefficients of satellites with concave geometries: comparing models and observations. *J. Spacecr. Rockets* **48**(2), 312–325 (2011). <https://doi.org/10.2514/1.50915>. ((ISSN 0022-4650))
49. Romano, F., Espinosa-Orozco, J., Pfeiffer, M., Herdrich, G., Crisp, N.H., Roberts, P.C.E., Holmes, B.E.A., Edmondson, S., Haigh, S., Livadiotti, S., Macario-Rojas, A., Oiko, V.T.A., Sinpetru, L.A., Smith, K., Becedas, J., Sullioti-Linner, V., Bisgaard, M., Christensen, S., Hanessian, V., Kauffman Jensen, T., Nielsen, J., Chan, Y.-A., Fasoulas, S., Traub, C., García-Almiñana, D., Rodríguez-Donaire, S., Sureda, M., Kataria, D., Belkouchi, B., Conte, A., Seminari, S., Villain, R.: Intake design for an atmosphere-breathing electric propulsion system (ABEP). *Acta Astron.* **187**, 225–235 (2021). <https://doi.org/10.1016/j.actaastro.2021.06.033> (ISSN 00945765)
50. Romano, F., Chan, Y.-A., Herdrich, G., Traub, C., Fasoulas, S., Roberts, P.C.E., Smith, K., Edmondson, S., Haigh, S., Crisp, N.H., Oiko, V.T.A., Worrall, S.D., Livadiotti, S., Huyton, C., Sinpetru, L.A., Straker, A., Becedas, J., Domínguez, R.M., González,

- D., Cañas, V., Sullioti-Linner, V., Hanessian, V., Mølgaard, A., Nielsen, J., Bisgaard, M., Garcia-Almiñana, D., Rodriguez-Donaire, S., Sureda, M., Kataria, D., Outlaw, R., Villain, R., Perez, J.S., Conte, A., Belkouchi, B., Schwalber, A., Heißerer, B.: RF helicon-based inductive plasma thruster (IPT) design for an atmosphere-breathing electric propulsion system (ABEP). *Acta Astron.* **176**, 476–483 (2020). <https://doi.org/10.1016/j.actaastro.2020.07.008> (ISSN 00945765)
51. Roberts, P.C.E., Crisp, N.H., Edmondson, S., Haigh, S.J., Lyons, R.E., Oiko, V.T.A., Macario-Rojas, A., Smith, K.L., Becedas, J., González, G., Vazquez, I., Brana, A., Antonini, K., Bay, K., Ghizoni, L., Jungnall, V., Morsbol, J., Binder, T., Boxberger, A., Herdrich, G.H., Romano, F., Fasoulas, S., Garcia-Almiñana, D., Rodriguez-Donaire, S., Kataria, D., Davidson, M., Outlaw, R., Belkouchi, B., Conte, A., Perez, J.S., Villain, R., Heißerer, B., Schwalber, A.: DISCOVERER—radical redesign of earth observation satellites for sustained operation at significantly lower altitudes. In: 68th International Astronautical Congress, number September, pp. 1–9, Adelaide, Australia (2017). International Astronautical Federation (IAF)
  52. Peter C.E. Roberts, Nicholas H. Crisp, Francesco Romano, Georg H. Herdrich, Vitor T.A. Oiko, Steve Edmondson, Sarah J. Haigh, Claire Huyton, Sabrina Livadiotti, Rachel E. Lyons, Katharine L. Smith, Luciana A. Sinpetru, Alastair Straker, Stephen D. Worrall, Jonathan Becedas, Rosa María Domínguez, David González, Valentín Cañas, Virginia Hanessian, Anders Mølgaard, Jens Nielsen, Morten Bisgaard, Adam Boxberger, Yung-An Chan, Stefanos Fasoulas, Constantin Traub, Daniel Garcia-Almiñana, Silvia Rodriguez-Donaire, Miquel Sureda, Dhiren Kataria, Ron Outlaw, Badia Belkouchi, Alexis Conte, Jose Santiago Perez, Rachel Villain, Barbara Heißerer, and Ameli Schwalber. DISCOVERER - Making Commercial Satellite Operations in Very Low Earth Orbit a Reality. In *70th International Astronautical Congress*, pages 1–9, Washington, DC, 2019. International Astronautical Federation (IAF)
  53. Oiko, V.T.A., Roberts, P.C.E., Edmondson, S., Worrall, S.D., Kataria, D., Outlaw, R., Haigh, S., Crisp, N.H., Lyons, R.E., Livadiotti, S., Huyton, C., Sinpetru, L.A., Becedas, J., González, G., Domínguez, R.M., González, D., Ghizoni, L., Jungnell, V., Bay, K., Morsbøl, J., Herdrich, G.H., Romano, F., Binder, T., Boxberger, A., Fasoulas, S., Traub, C., Garcia-Almiñana, D., Rodriguez-Donaire, S., Sureda, M., Villain, R., Perez, J.S., Conte, A., Belkouchi, B., Schwalber, A., Heißerer, B.: Design and development of a hyper-thermal atomic oxygen wind tunnel facility. In: 14th ISMSE and 12th ICPMSE, Biarritz, France (2018), pp. 1–6. <https://doi.org/10.1299/jsmemag.121.119842>
  54. Oiko, V.T.A., Roberts, P.C.E., Worrall, S.D., Edmondson, S., Haigh, S.J., Crisp, N.H., Livadiotti, S., Huyton, C., Lyons, R.E., Smith, K.L., Sinpetru, L.A., Holmes, B.E., Becedas, J., Domínguez, R.M., González, D., Cañas, V., Hanessian, V., Mølgaard, A., Nielsen, J., Bisgaard, M., Boxberger, A., Chan, Y.-A., Herdrich, G.H., Romano, F., Fasoulas, S., Traub, C., Garcia-Almiñana, D., Rodriguez-Donaire, S., Sureda, M., Kataria, D., Outlaw, R., Belkouchi, B., Conte, A., Perez, J.S., Villain, R., Heißerer, B., Schwalber, A.: A ground-based experimental facility for orbital aerodynamics research. In: 70th International Astronautical Congress, Washington, DC, 2019, pp. 1–7. International Astronautical Federation (IAF)
  55. Crisp, N.H., Roberts, P.C.E., Livadiotti, S., Macario Rojas, A., Oiko, V.T.A., Edmondson, S., Haigh, S.J., Holmes, B.E.A., Sinpetru, L.A., Smith, K.L., Becedas, J., Domínguez, R.M., Sullioti-Linner, V., Christensen, S., Nielsen, J., Bisgaard, M., Chan, Y.-A., Fasoulas, S., Herdrich, G.H., Romano, F., Traub, C., García-Almiñana, D., Rodríguez-Donaire, S., Sureda, M., Kataria, D., Belkouchi, B., Conte, A., Seminari, S., Villain, R.: In-orbit aerodynamic coefficient measurements using SOAR (Satellite for Orbital Aerodynamics Research). *Acta Astron.* **180**, 85–99 (2021). <https://doi.org/10.1016/j.actaastro.2020.12.024> (ISSN 00945765)
  56. Llop, J.V., Roberts, P.C.E.: ΔDsat, a QB50 CubeSat mission to study rarefied-gas drag modelling. *Acta Astron.* **89**, 130–138 (2013). <https://doi.org/10.1016/j.actaastro.2013.04.006>. (ISSN 00945765)
  57. Crisp, N.H., Livadiotti, S., Roberts, P.C.E., Edmondson, S., Haigh, S.J., Huyton, C., Lyons, R.E., Oiko, V.T.A., Smith, K.L., Sinpetru, L.A., Straker, W., Stephen, D., Becedas, J., Domínguez, R.M., González, D., Cañas, V., Hanessian, V., Mølgaard, A., Nielsen, J., Bisgaard, M., Boxberger, A., Chan, Y.-A., Herdrich, G.H., Romano, F., Fasoulas, S., Traub, C., Garcia-Almiñana, D., Rodriguez-Donaire, S., Sureda, M., Kataria, D., Outlaw, R., Belkouchi, B., Conte, A., Perez, J.S., Villain, R., Heißerer, B., Schwalber, A.: Demonstration of aerodynamic control Manoeuvres in very low earth orbit using SOAR (Satellite for Orbital Aerodynamics Research). In: 70th International Astronautical Congress, Washington, DC (2019). International Astronautical Federation (IAF)
  58. Livadiotti, S., Crisp, N.H., Roberts, P.C.E., Edmondson, S., Haigh, S.J., Huyton, C., Lyons, R.E., Oiko, V.T.A., Smith, K.L., Sinpetru, L.A., Straker, A., Worrall, S.D., Becedas, J., Domínguez, R.M., González, D., Cañas, V., Hanessian, V., Mølgaard, A., Nielsen, J., Bisgaard, M., Boxberger, A., Chan, Y.-A., Herdrich, G.H., Romano, F., Fasoulas, S., Traub, C., Garcia-Almiñana, D., Rodriguez-Donaire, S., Sureda, M., Kataria, D., Outlaw, R., Belkouchi, B., Conte, A., Perez, J.S., Villain, R., Heißerer, B., Schwalber, A.: Concepts and applications of aerodynamic attitude and orbital control for spacecraft in very low earth orbit. In: 70th International Astronautical Congress, Washington, DC, 2019. International Astronautical Federation (IAF)
  59. Llop, J.V., Roberts, P.C.E., Hao, Z.: Using the attitude response of aerostable spacecraft to measure thermospheric wind. *CEAS Space J* (2017). <https://doi.org/10.1007/s12567-017-0153-9>. (ISSN 1868-2502)
  60. Greaves, J.C., Linnett, J.W.: The recombination of oxygen atoms at surfaces. *Trans. Faraday Soc.* **54**, 1323 (1958). <https://doi.org/10.1039/tf9585401323>. (ISSN 0014-7672)
  61. Greaves, J.C., Linnett, J.W.: Recombination of atoms at surfaces. Part 6.—recombination of oxygen atoms on silica from 20°C to 600°C. *Trans. Faraday Soc.* **55**, 1355–1361 (1959). <https://doi.org/10.1039/TF9595501355> (ISSN 0014-7672)